

Robustness of Kappa (κ) Measurement in Low-to-Moderate Seismicity Areas: Insight from a Site-Specific Study in Provence, France

by Vincent Perron,^{*} Fabrice Hollender,[†] Pierre-Yves Bard, Céline Gélis, Cédric Guyonnet-Benaize, Bruno Hernandez, and Olga-Joan Ktenidou

Abstract Determination of the site component of κ (κ_0) is important in the implementation of host-to-target adjustments for estimation of seismic hazard at hard-rock sites. Its evaluation through the classical approach of [Anderson and Hough \(1984\)](#), κ_{0_AS} , faces specific difficulties in low-to-moderate seismicity areas because the quantity and bandwidth of the usable data are generally limited. In such a context, measurements might have higher sensitivity to site amplification, frequency-dependent attenuation, the earthquake source, and the instrumental equipment. Here, the κ_{DS} (displacement spectrum) approach of [Biasi and Smith \(2001\)](#) is compared with the κ_{AS} (acceleration spectrum) approach for three sites in an industrial area in Provence (southeastern France). A semiautomatic procedure is developed to measure individual values of κ_r that reduce interoperator variability and provide the associated uncertainty. We show that this uncertainty is mainly dependent on the bandwidth used to determine κ_r . A good agreement is found between κ_{0_AS} and κ_{0_DS} for the two hard-rock sites, which yield ~ 30 ms. This highlights the κ_{DS} approach that is well adapted to low-magnitude events recorded at rock sites, and the use of velocimeters in low-to-moderate seismicity areas. The comparisons between these approaches are also used to infer the reliability of κ measurements by addressing their sensitivity to site amplification, frequency-dependent attenuation, and the earthquake source. First, the impact of site amplification on κ_0 estimates is shown to be very important and strongly frequency-dependent for stiff-soil sites, and non-negligible for hard-rock sites. Second, frequency-dependent attenuation cannot be ruled out for κ , as indicated by comparison with the literature quality factor (Q) for the Alps. Finally, a source component for κ_{AS} is questionable from the comparison of κ_{r_AS} evaluated for a cluster of events that shared the same path and site components.

Introduction

The kappa (κ) parameter describes the high-frequency spectral shape of ground motion. This parameter was introduced by [Anderson and Hough \(1984\)](#) as the linear decay in a log-linear space of the acceleration high-frequency Fourier amplitude spectrum (FAS) of the horizontal component of the shear waves. For a given record at epicentral distance (R_e), κ (denoted κ_r) can be defined as

$$A(f) = A_0 \exp(-\pi\kappa_r f), f_1 < f < f_2, \quad (1)$$

in which f_1 and f_2 are the frequency bounds between which the decay of the spectrum amplitude ($A(f)$) is approximately

linear in a log-linear space. κ_r can be decomposed in terms of site (κ_0), source (κ_S), and path ($\bar{\kappa}$) components:

$$\kappa_r = \kappa_0 + \kappa_S + \bar{\kappa}(R_e). \quad (2)$$

[Anderson and Hough \(1984\)](#) assumed that κ_r can only be explained by the attenuation of the path and the site when it is measured above the corner frequency (f_c); that is, where the acceleration spectrum of the source is assumed to be flat in the [Brune \(1970\)](#) model. This ω^{-2} source model was initiated by [Aki \(1967\)](#) and remains a reference model to date. According to the original model that neglected the source component ($\kappa_S = 0$), the distance-independent part of κ_r was attributed to κ_0 ; that is, to the S -wave attenuation due to the geological structure beneath the recording site ([Hanks, 1982](#); [Anderson and Hough, 1984](#); [Hough and Anderson, 1988](#)). The distance-dependence term that represents the attenuation

^{*}Also at University of Grenoble Alpes, ISTerre, CNRS, IRD, IFSTTAR, F-38000 Grenoble, France; and at IRSN, PRP-DGE/SCAN/BERSSIN, BP 17, F-92262 Fontenay-aux-Roses, France.

[†]Also at University of Grenoble Alpes, ISTerre, CNRS, IRD, IFSTTAR, F-38000 Grenoble, France.

of the S wave along the propagation in the crust from the source to the site can be described by many different models. Generally, the linear assumption $\bar{\kappa}(R_e) = m_\kappa \times R_e$ proposed by Anderson and Hough (1984) is a reasonable approximation (Douglas *et al.*, 2010; Ktenidou *et al.*, 2013). Then, when the source term is neglected, equation (2) can be written as

$$\kappa_r(R_e) = \kappa_0 + m_\kappa \times R_e. \quad (3)$$

In this model, the site term κ_0 and the path term m_κ (following the notation of Douglas *et al.*, 2010) can be simply separated by linear regression, in which the first term is the intercept at zero epicentral distance ($\kappa_r(0)$), and the second term is the slope of the $\kappa_r(R_e)$ linear trend with epicentral distance. In equation (3), κ_r and κ_0 are expressed in seconds (s), whereas m_κ is expressed in s/m, with the epicentral distance R_e expressed in meters.

The site component κ_0 has many applications in hazard seismology because it helps to constrain the high-frequency spectral shape of the predicted seismic signals at a specific site. This is particularly important for low-attenuating hard-rock sites, where the ground motion can be underestimated at high frequencies. κ_0 has thus been used as an input parameter in stochastic simulations (Boore, 1986, 2003; Beresnev and Atkinson, 1997; Graves and Pitarka, 2010) and in the functional forms of some ground-motion prediction equations (GMPEs; e.g., Anderson *et al.*, 1996; Laurendeau *et al.*, 2013). However, the vast majority of GMPEs are developed using data from accelerometric networks in seismically active regions. Thus, the representativeness of the GMPEs for hard-rock sites is not ensured because surface accelerometric stations are rarely installed on hard-rock sites. The host-to-target adjustments take into account differences in site properties (i.e., for the time-averaged V_S within the first 30 m [V_{S30}] and κ_0) to adapt the GMPEs from the host soft rock or rock where they are developed to the target hard-rock sites where they are needed (Campbell, 2003, 2004; Cotton *et al.*, 2006; Van Houtte *et al.*, 2011; Delavaud *et al.*, 2012; Ameri *et al.*, 2017; Boore and Campbell, 2017). Although an estimation of κ_0 is very often available in active host areas, its determination is more difficult in target areas of low-to-moderate seismicity. When no seismological recordings are available, κ_0 is generally deduced from the κ_0/V_{S30} correlation, even if the scatter of this correlation is very large. However, this introduces large uncertainties in seismic-hazard assessments. It is thus of great interest to determine reliable site-specific values of κ_0 from seismic recordings, which can be relatively challenging in low-to-moderate seismicity areas.

Since the first definition of κ by Anderson and Hough (1984), many studies have proposed different techniques to determine κ_r or κ_0 . Ktenidou *et al.* (2014) provided a comprehensive review of the methods at the time and provided the notations that are followed here. The evaluation of κ_0 through the original definition based on the acceleration spectrum (κ_{0_AS}) is difficult in low-seismicity areas because of the lack of local earthquakes with magnitudes > 3 .

Indeed, the lower the magnitude, the higher the f_c and the lower the highest frequency with good signal-to-noise ratio ($\text{SNR} > 3$), which leads to a smaller usable width of the frequency window ($\Delta f = f_2 - f_1$) for the κ_{r_AS} measurement. Because of this difficulty, only one study has explicitly reported an estimation of κ_{0_AS} for mainland France (Douglas *et al.*, 2010), and to do so, they joined the individual κ_{r_AS} measured from many sites of the same type and in the same region.

The approach proposed by Biasi and Smith (2001) represents an alternative for low-seismicity areas that estimates κ_{r_DS} (displacement spectrum), and then κ_{0_DS} , on the horizontal components of the FAS computed from the direct shear-wave part of the displacement seismogram. The displacement spectrum of the source flattens up to f_c , which allows the measurement of κ_{r_DS} for low-magnitude events and at lower frequencies (i.e., below f_c). This relies on the assumption that the stress drops for the smallest earthquakes are similar to those of the large earthquakes, which implies high f_c values (Kilb *et al.*, 2012). In contrast to κ_{r_AS} , the lower the magnitude of the earthquake, the larger the Δf for the measure of κ_{r_DS} on the record. This is why this approach was initially proposed for very small magnitude events ($M < 1$). Finally, local-to-regional earthquakes ($R_e < 200$ km) listed in the catalog for low-to-moderate seismicity areas have magnitudes mainly between 1 and 3, which is not in the ideal magnitude range for either the κ_{AS} or κ_{DS} approaches. This difficulty can lead to higher sensitivity of the results to the site amplification, the frequency-dependent attenuation, and the earthquake source, due to the small Δf that are used for κ_{r_AS} and κ_{r_DS} .

Indeed, because the physics of κ is not clear, and wide uncertainty is generally associated with its measurement, this also results in a multiplicity of possible interpretations. The renewal of interest in this parameter over the last decade has recently led to numerous studies of its dependence on various parameters and to a reduction in the associated uncertainties (Campbell, 2009; Van Houtte *et al.*, 2011; Kilb *et al.*, 2012; Ktenidou *et al.*, 2013, 2015; Edwards *et al.*, 2015; Parolai *et al.*, 2015). First, since the origins of κ , some studies have attributed part of the decay to source effects (Papageorgiou and Aki, 1983; Aki, 1987; Papageorgiou, 1988, 2003; Gariel and Campillo, 1989), whereas a few studies have suggested that there might be both source and site components for κ_r (Tsai and Chen, 2000; Purvance and Anderson, 2003). Although the site-effect interpretation is commonly accepted at present, and the majority of recent studies of κ neglect the source term, an influence of the source on κ_r is likely if there is any divergence from the ω^{-2} source model. Moreover, the f_c criterion that allows for the neglecting of the source influence is difficult to respect, as its estimation is very uncertain, especially when the value of the stress drop for the target region is not known. Second, one of the most dubious assumptions concerning κ is its frequency independence. This assumption is an implicit part of the choice of a linear model to measure κ_r between f_1 and f_2 of the acceleration spectrum

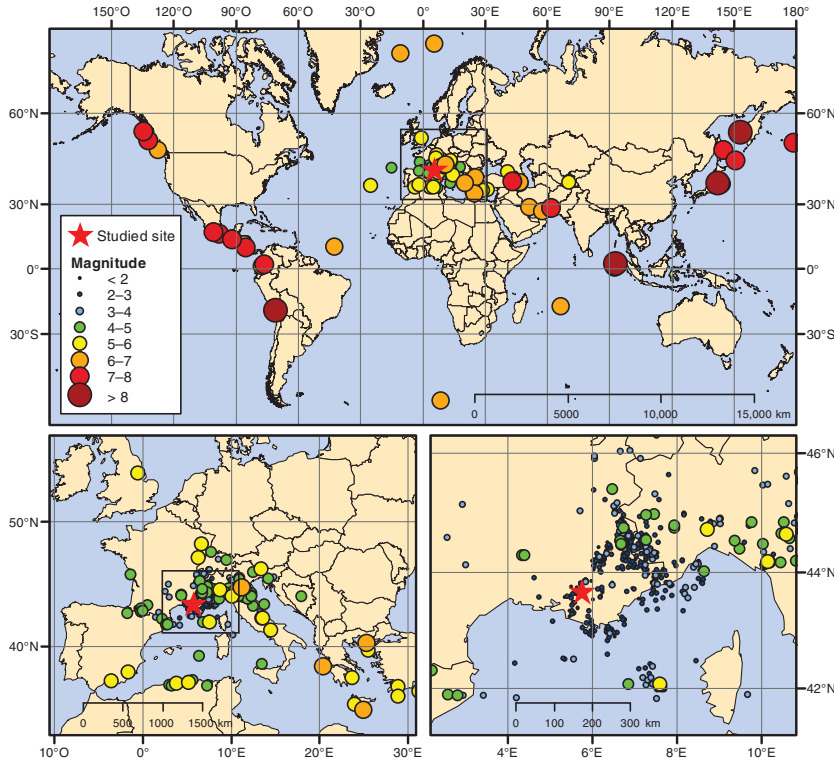


Figure 1. Maps of the earthquake epicenters recorded at the studied site (red star), at three different scales.

(equation 1). κ_r is tied to another attenuation parameter, the effective quality factor of the S wave Q_{ef} (Futterman, 1962; Knopoff, 1964). Campbell (2009) provided a good overview of the relationship between Q and κ . Since Q_{ef} was introduced, it has been widely accepted as frequency dependent at least in part. The model proposed by Aki (1980) and Dainty (1981) divided Q_{ef} into two parts: a frequency-independent intrinsic attenuation part (Q_i) and a frequency-dependent scattering part (Q_{sc}), given as follows:

$$\frac{1}{Q_{ef}} = \frac{1}{Q_i} + \frac{1}{Q_{sc}}. \quad (4)$$

Based on the frequency-dependent t^* model of Cormier (1982), Hough *et al.* (1988) and Hough and Anderson (1988) linked Q and κ with a general frequency-independent model. This model described the attenuation along the ray path as

$$\kappa_r(r) = \int_{\text{path}} \frac{1}{Q_i(z)V_S(z)} dr, \quad (5)$$

in which $Q_i(z)$ is the frequency-independent component of Q_{ef} , and V_S is the shear-wave velocity at depth z within the profile. This model assumes that Q_i and V_S are laterally homogeneous and that Q_{sc} does not affect the evaluation of κ when it is inversely proportional to the frequency (Warren, 1972; Rovelli, 1982; Anderson, 1986). However, the frequency-independence assumption for κ is dubious, because depending on the size of the heterogeneities, a frequency-

dependent scattering contribution cannot be excluded (Edwards *et al.*, 2015; Ktenidou *et al.*, 2015; Parolai *et al.*, 2015). This might impact upon κ , depending on the frequency band in which it is defined, which will lead to different results when using different approaches (e.g., high-frequency κ_{AS} , low-frequency κ_{DS} , and κ_{BB} broadband inversion). Finally, another frequency-dependent phenomenon can modify the spectrum and therefore the evaluation of κ : the site amplification. Indeed, the spectral modulations induced by site effects can change the slope of the decay and thus modify the κ_r estimates, depending on the selected frequency windows. Moreover, the modification of the spectrum shape can hide the frequency interval in which the decay should be linear in the absence of site amplification, and thus alter the identification of the true frequency band in which κ_r should be measured (Hough *et al.*, 1999; Parolai and Bindi, 2004; Van Houtte *et al.*, 2014; Edwards *et al.*, 2015). The smaller the Δf , the greater the influence of the site amplification on κ should be.

The objective of the present study is to evaluate the applicability of reliable determination of site-specific κ in the low-to-moderate seismic context of mainland France. After a short description of the study area in terms of its geology and the datasets, some recommendations are provided for implementation of the instrumentation, and the site effects are evaluated. First, the semiautomatic procedure used to measure κ_r is introduced, and a detailed comparison is given between the κ_{AS} and κ_{DS} approaches on hard-rock sites. Second, the sensitivity of κ to frequency-dependent attenuation, site amplification, and the earthquake source are investigated. Finally, the reliability and variability of the κ measurements are discussed in the context of low-to-moderate seismicity areas.

Study Area and Datasets

Study Area

The industrial area under study is in Provence, close to the Alps (southeastern France), near the town of Saint-Paul-Lez-Durance. The Alps is one of the most active seismic regions in mainland France, although the associated seismic activity is low to moderate (Guéguen *et al.*, 2007; Sanchez *et al.*, 2010). Figure 1 shows the location of the study site and the event epicenters from the database used. The main database is composed of seismic data that were recorded between February 2012 and June 2014, with the recording of nearly 500 earthquakes by several velocimeters (Güralp CMG-6TD). During this two-year period, two seismic sequen-

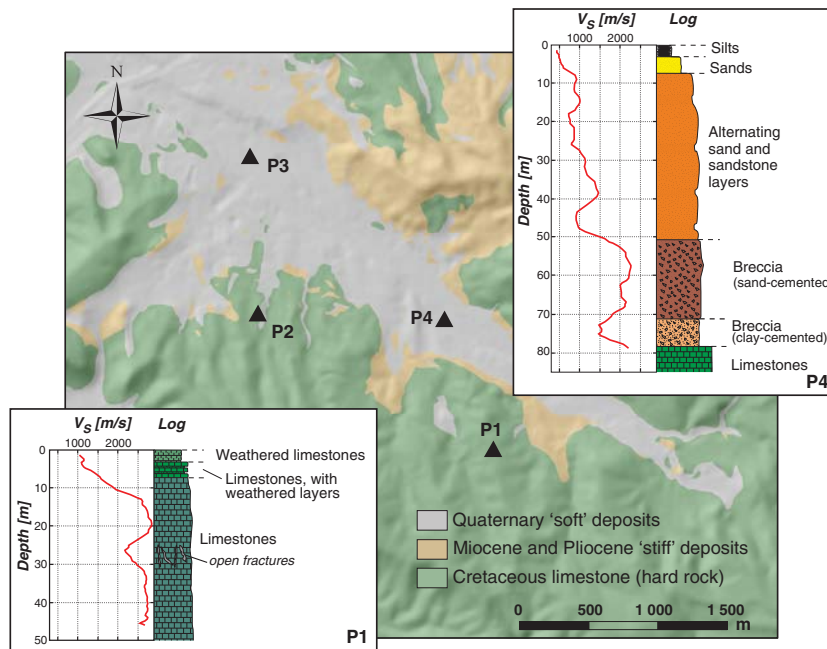


Figure 2. Geological map of the recording area. Sites P1 and P2 are located on hard rock, whereas sites P3 and P4 are located on stiff soils. At sites P1 and P4, boreholes allowed the recording of the velocity profiles with depth (V_S , V_P) for different techniques such as the crosshole, downhole, and P - S suspension logging methods.

ces occurred, after the 26 February 2012 M_L 4.5 and 7 April 2014 M_L 5.2 earthquakes of Jausiers. These two sequences are approximately collocated at $R_e = 120$ km and at an $\sim N50^\circ E$ azimuth from the recording area (Fig. 1). In the framework of this κ study, only the three sites where the seismic records are the most abundant are considered (Fig. 2; P1, P2, and P3). Sites P2 and P3 have two accelerometers (Güralp CMG-5TDE) as well as the velocimeters. All of the sensors record continuously with a 100-Hz sampling frequency and a flat response beyond the Nyquist frequency (50 Hz). Seismic events were extracted from the continuous data using the earthquake bulletin information provided mainly by the European-Mediterranean Seismological Centre. When information was missing for an earthquake, the information used was from the Réseau National de Surveillance Sismique (French National Seismic Surveillance Network), Géoazur, or the Italian Seismological Instrumental and Parametric Database. These catalogs were also used to determine the earthquake parameters (e.g., magnitude, location, among others), where the magnitudes were mainly local (M_L). Two accelerometers in triggering mode completed the database, with 300 additional events recorded from 2000 to 2011 at sites P2 and P3. This initial instrumentation was managed by the Laboratory for Detection and Geophysics (French Alternative Energies and Atomic Energy Commission [CEA], France), which also provided the associated earthquake parameters. Differences between the catalogs are assumed to be negligible compared to the uncertainty associated with κ . Finally, more than 800 events were recorded, with epicentral distances from 3 to $> 10,000$ km. Some teleseisms were also recorded, although the vast major-

ity of events were within epicentral distances of 500 km. All of the recorded regional earthquakes were crustal events (depth < 30 km) and corresponded to weak motions. Almost all of these had local magnitudes < 4 and were northeast of the recording site. However, the number of events recorded by each site varied due to differences in the recording durations, and this was very dependent on the application (Table 1). For κ estimation, only the best records from the closest events ($R_e < 180$) were used to provide good SNRs over a broad enough frequency band, and to ensure that the propagation is only in the crust.

Sites P1 and P2 are located on outcropping massive Cretaceous limestone. Site P3 and a further site, site P4, are located within a relatively small paleovalley (a few hundred meters wide, 50–150 m deep) that is filled with stiff Miocene sand and sandstone and softer quaternary deposits. Based on the geophysical measurements for sites P1, P2, P3, and P4, V_{S30} is evaluated at 2100, 1800, 440, and 720 m/s, respectively. Sites P1 and P2 are thus classified as the hard-rock class, whereas sites P3 and P4 are in the very dense soil class, according to the *National Earthquake Hazards Reduction Program* classification. The sensor at site P1 is set up in a seismic vault buried at 3 m in depth, whereas the sensors of sites P2, P3, and P4 are at the surface. Figure 2 shows the locations of these four sites on a simplified geological map. For sites P1 and P4, three cored boreholes had been drilled, which provided a lithological description of the substratum, as well as *in situ* shear-wave velocity measurements performed using crosshole, downhole, and P - S suspension logging methods. Site P1 was one of the sites used by the InterPACIFIC project to perform a comparative benchmark of invasive and noninvasive methods for site characterization (Garofalo *et al.*, 2016). No κ evaluation was carried out for site P4, due to too low a number of well-recorded seismic events. However, site P4 is included here due to the availability of borehole and *in situ* V_S measurements, which are representative of the local basin features.

Spectrum Computation

The FAS are mandatory to compute κ_r and for site-effect assessment through horizontal-to-vertical spectral ratio and standard spectral ratio (SSR) approaches. A common procedure was followed to determine the FAS from the earthquake recordings (Perron *et al.*, 2017). A visual check and manual picking of the P -wave and S -wave first arrivals (T_p , T_s) were performed for one site of the network (generally P1) for each earthquake. It is assumed that the

Table 1

Number of Events Available According to the Sites (P1–P4) and to the Application: Standard Spectral Ratio (SSR), κ Measure on the Acceleration (κ_{AS}), or Displacement (κ_{DS}) Spectrum

Site	Number of Events Available			
	Total	For the SSR/P1	For κ_{AS}	For κ_{DS}
P1	453	—	33	37
P2	678	371	35	39
P3	686	350	48	18
P4	246	205	—	—

differences in the time arrivals between these sites are negligible due to the very short interstation distances compared to the epicentral distances. In addition to T_p and T_S , the end of the signal (T_{end}) was also visually picked, based on a time-frequency analysis (spectrograms), to take into consideration the SNR criteria and to detect potential postevent perturbations at every frequency (e.g., aftershocks, transient noise, among others). Only the direct S -wave window was considered for κ estimation, whereas the entire signal was used to assess the SSR. A 5% cosine taper was applied at the edge of each time window, and the windows were extended to apply the cosine taper out of the target window. The S -wave duration was defined by a specific, and relatively simple, scheme (Perron *et al.*, 2017) that took into account the expansion due to the propagation (approximated by $T_S - T_p$) and the source (through $1/f_c$). In the low-to-moderate seismicity context of Provence, the S -wave window is mainly controlled by the propagation term, because the source term is negligible for magnitudes < 5 . A minimum nominal duration of 5 s was used to constrain the spectral resolution at low frequencies. The influence of window length on the spectrum was tested, which led to only small changes, in agreement with previous observations (Anderson and Hough, 1984; Tsai and Chen, 2000; Douglas *et al.*, 2010). To obtain length-independent FAS, the Fourier transforms were normalized by the square root of the number of samples, which led to the computation of the FAS density (FASD). The FASD is important only for the SNR computation when the noise and the signal windows are not of the same duration. The north–south and east–west components were combined to obtain a single orientation-independent component, as follows:

$$S(H) = \frac{S(N + iE)}{\sqrt{2}}. \quad (6)$$

This evaluation of the horizontal mean component is equivalent to the quadratic mean in the frequency domain [$S(H) = \sqrt{(S(E)^2 + S(N)^2)/2}$]. Nevertheless, this complex representation of horizontal motion allowed it to be applied to the time domain and maintained the phase between the components (Steidl *et al.*, 1996). A criterion of a minimum of ten wavelengths contained in the signal was applied to define the minimum frequency (f_{min}), which is determined according to the duration of the time window (Δt): $f_{min} =$

$10/\Delta t$. For κ_{AS} or κ_{DS} , the spectra (in acceleration or displacement) were obtained from the velocity spectra by multiplication or division by $2\pi if$ in the Fourier domain.

Velocimeter versus Accelerometer

Because there is colocalization of accelerometers with velocimeters at sites P2 and P3, these data were used for comparisons between these two types of sensors, in terms of the quantity and quality of the records. The quality of a dataset impacts directly on the achievability of the κ measurement. Figure 3 shows the comparison between the number of accelerometer and velocimeter recordings that satisfied similar quality criteria at the same rock site (site P2) over the same period of time. The quality criteria are based on the SNR at each frequency and for each recording, with different threshold values considered for the SNR (i.e., 3, 10, and 50). Figure 3 thus shows the percentages of the recorded events for which the (frequency-dependent) SNR falls within the corresponding ranges (i.e., $SNR < 3$; $3 \leq SNR < 10$; $10 \leq SNR < 50$; $SNR \geq 50$). This shows that the velocimeter recordings provide more to many more usable events, especially below 20 Hz (sometimes > 50 -fold for $10 \leq SNR < 50$), and the available frequency ranges are mainly from 0.25 to 15 Hz, which is below the high-frequency range generally required for κ_{AS} . Above 15 Hz, the two types of sensors give similar results, even if the number of recorded events with $SNR > 3$ is relatively low due to the lack of local earthquakes. It should be noted, however, that these data were obtained for a given accelerometer model versus a given velocimeter model, because the purpose here is not to achieve complete instrumental comparisons. However, although the use of accelerometers is justified for strong ground motion recordings (because they do not saturate), these experimental results demonstrate the interest in using velocimeters for site-specific studies in low-to-moderate seismicity areas, to record enough earthquakes within a reasonable time period. If only accelerometers were available, only a few κ_r and no κ_0 evaluations would have been possible for this study, especially for κ_{DS} , which was evaluated mainly at low frequencies (i.e., below 15 Hz).

Site Amplification

Seismic ground motion can be modified (most often amplified) by the near-surface geological structure anywhere at the Earth surface. This phenomenon is referred to as the site effects, which have been widely observed for alluvial deposits, with amplitudes and frequency bands that vary greatly from site to site as a function of their geometry and mechanical properties. However, it is often neglected for hard-rock sites, because their amplitude is expected to be much lower and to be shifted to high frequencies only (i.e., beyond 5–10 Hz). These frequency-dependent phenomena have to be evaluated on a site-specific basis, because they might significantly contaminate the measurement of κ_r , based on the apparent spectral slope.

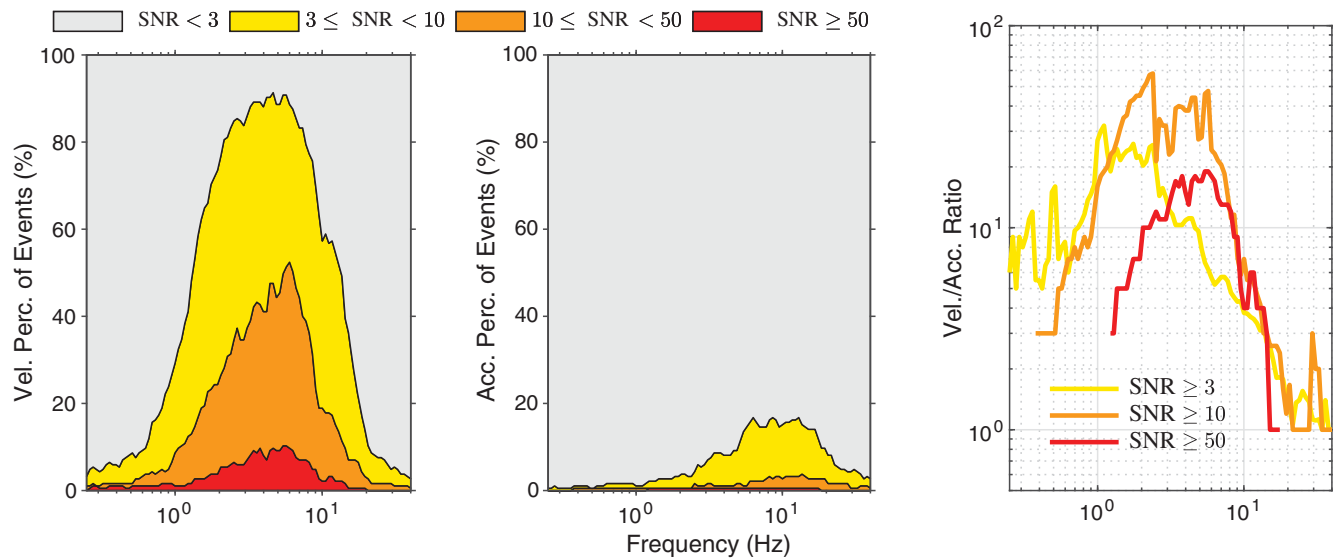


Figure 3. Comparisons of the percentage of (left) velocimeter and (middle) accelerometric recordings that satisfy four ranges of signal-to-noise ratios (SNRs) as a function of the frequency. Both instruments recorded in continuous mode, at the same site (P2), and over the same period of time. The S -wave windows from a total of 185 earthquakes were considered. (Right) The ratio between these velocimeter and accelerometer recordings that satisfy the same SNR criteria.

The records of numerous earthquakes for each site allow the inference of the relative transfer function using the SSR approach (Borcherdt, 1970). One important precondition for using the SSR technique is the availability of a nearby reference (i.e., rock) site with negligible site effects. This approach consists of computing the ratio between the FAS from the earthquake recorded at both the site and the reference site. The FAS were processed following the procedure described in the Spectrum Computation section and were smoothed following the Konno and Ohmachi (1998) procedure, with a b -value of 30. For each frequency, the median was estimated from all of the earthquakes with $\text{SNR} > 3$. Figure 4 shows the SSR data for the mean horizontal components and the vertical components for sites P2, P3, and P4, using P1 as the reference site. The theoretical 1D site transfer function at P1 is shown in Figure 4 (black dashed curves). This transfer function was computed with a velocity profile that used the measured velocity profile down to 46 m, in which V_S reached ~ 2800 m/s (Fig. 2). This was then completed down to 8 km in depth ($V_S = 3600$ m/s), with a generic velocity profile to account for crustal amplification. The 1D reflectivity model (Kennett, 1974) was used to reproduce the response of horizontally stratified layers excited by a vertically incident SH plane wave. An infinite Q was used for the computation to consider only the site amplification.

Site P3 shows significant site amplification above 2 Hz (e.g., up to 12-fold at 7 Hz on the horizontal component), whereas site P4 shows more moderate amplification (up to fivefold at 4 Hz). These amplifications appear to be mostly related to the first 55 m of soil, according to the V_S profile shown in Figure 2. According to the P2/P1 SSR, as well as the theoretical 1D transfer function computed at site P1, the

amplification at the rock sites is much lower. This is due to the weathered zone that affects the limestone within the first few meters beneath the surface.

In addition to these lithographic effects, the topography of the free surface near the site can also modify the spectral shape, and thus the evaluation of κ_r , especially on rock sites where the lithographic effects are limited and the topography is important. However, negligible influence of the topography was noted for each site through the frequency-scaled curvature approach proposed by Maufroy *et al.* (2015).

Kappa

Data Processing

Once the horizontal mean FAS or FASD have been processed (equation 6), κ_r can be determined following the methodology proposed by Ktenidou *et al.* (2013). The slope of the spectral decay is measured by the linear regression from the acceleration FAS for κ_{r_AS} and from the displacement FAS for κ_{r_DS} . An example of the κ_{r_AS} measurements is given in Figure 5. Care was taken to be sure that the frequency window within the slope that was measured had $\text{SNR} > 3$. In the same way, special attention was paid to the frequency window, to be sure that it was above f_c for κ_{r_AS} and below f_c for κ_{r_DS} . This f_c checking is essential for the assumption that the result is independent of the shape of the source spectrum in the Brune (1970) model. Direct visual evaluation of f_c was carried out on the displacement spectra of a few earthquakes, and comparisons were made with the value proposed by Drouet *et al.* (2010) for the Alps. Then, the initial bounds of the frequency window (f_{1ni} , f_{2ni}) were manually picked, respecting the SNR and f_c criterion, and for the most linear decay.

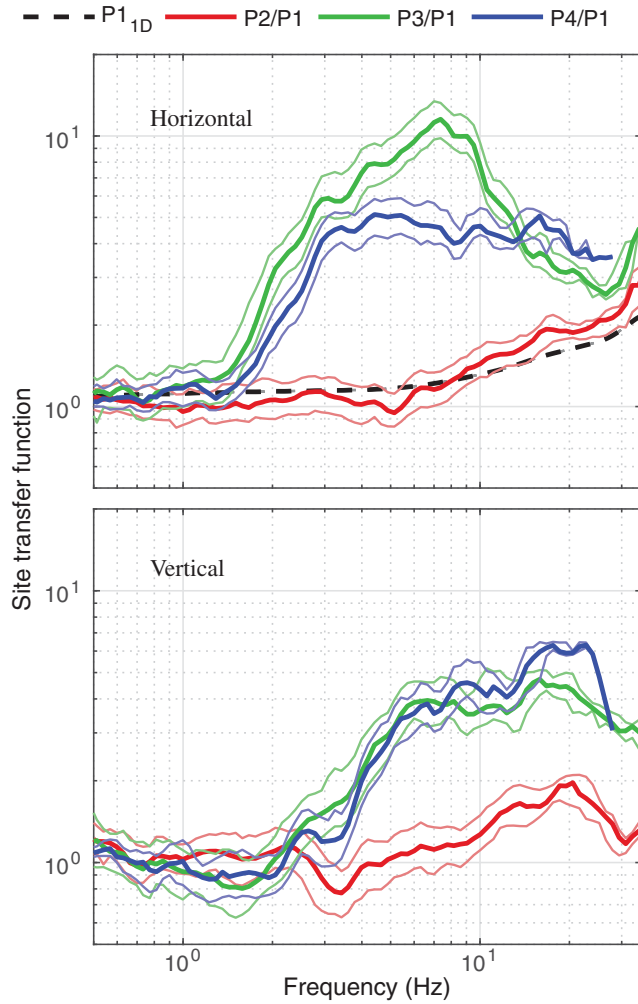


Figure 4. Median and percentile 16% and 84% of the standard spectral ratios (SSRs) estimated from the earthquakes recorded at sites P2 (red), P3 (green), and P4 (blue), according to the reference site P1, for (top) the horizontal mean and (bottom) the vertical components. The theoretical transfer function estimated from the velocity profile at site P1 is shown by the black dashed curve for the horizontal mean component.

A semiautomatic procedure was developed for more precise and repeatable selection of the lower and upper bounds (f_1, f_2) of this frequency window. The aim is to reduce the variability between operators and to determine the uncertainty associated with each measure of κ_r . This procedure is illustrated in Figure 5: an uncertainty range ($\delta f = \pm 2$ Hz) is defined around each bound of this manually selected frequency window (f_{1ini}, f_{2ini}), and κ_r is estimated from the linear regression slopes over all of the frequency interval combinations ($f_{1ini} \pm \varepsilon_1 \delta f, f_{2ini} \pm \varepsilon_2 \delta f$), with ε_1 and ε_2 as random numbers between 0 and 1 (Fig. 5, yellow lines). In this way, the precision of the κ_r estimate can be quantified with various statistical parameters (e.g., minimum, maximum, mean, and standard deviation). The best κ_r estimation is defined as that which minimizes the root mean square (rms):

$$\text{rms} = \sqrt{\frac{\sum_i (\text{FAS}(f_i) - \text{FAS}_{\text{fit}}(f_i))^2}{N}}, \quad f_1 \leq f_i \leq f_2, \quad (7)$$

in which $\text{FAS}(f_i)$ is the S -wave FAS, $\text{FAS}_{\text{fit}}(f_i)$ is the regression prediction at the i th frequency, and N is the number of samples between the f_1 and f_2 bounds of the tested slope. Only windows wider than 10 Hz were taken into account to ensure the minimum reliability for the κ_r estimation. Finally, the best-fit κ_r estimate (Fig. 5, red line) that minimizes rms is taken with its associated uncertainty, which corresponds to the difference between the maximum and minimum values of κ_r (Fig. 5, blue lines) obtained in the tested slope set ($\Delta\kappa_r = \kappa_{r_{\text{max}}} - \kappa_{r_{\text{min}}}$).

Once every κ_r had been estimated with their associated uncertainties, κ_0 was computed following the chosen distance-dependence model ($\kappa_r(R_e)$). Here, the simple linear regression (equation 3) was considered, with each κ_r value weighted by the inverse of its associated uncertainty. κ_0 can also be approximated by the individual κ_r measurements that correspond to short R_e distances, on the assumption that the path component is negligible when the earthquake occurs within a few tens of kilometers around the site (Ktenidou *et al.*, 2013). Thus, in addition to the classical κ_0 intercept value evaluation, another estimate $\kappa_{0 < 30 \text{ km}}$ was also computed as the mean of the κ_r values from events with $R_e < 30$ km. This approach avoids a too large sensitivity to the slope of the distance-dependence model, but it can lead to slightly higher κ_0 estimates.

Results and Comparison between κ_{AS} and κ_{DS}

The different κ definitions imply differences in the range of the magnitudes and frequencies that are considered for its computation. Figure 6 shows the distribution of events used to determine κ_r from the acceleration (Fig. 6, black filled circles) and displacement (Fig. 6, gray circles) FAS according to the magnitude, depth, and back azimuth. All of the events were crustal (depth < 20 km), and the back-azimuthal repartition shows preferential orientation close to N50°E for both of these approaches. In comparison with previous studies (Kilb *et al.*, 2012), events down to relatively low magnitudes for $\kappa_{r\text{-AS}}$ ($M < 3$) were used here, as well as relatively high magnitudes for $\kappa_{r\text{-DS}}$ ($M > 1.5$). However, for $\kappa_{r\text{-AS}}$, most of the events have magnitudes > 3 , and those that are < 3 are close enough to provide energy of 30 Hz or more, which allows for very high-frequency κ estimations.

For magnitudes between 2 and 3, these acceleration and displacement approaches have both been realized. A comparison of the data obtained with these approaches for two earthquakes is given in Figure 7. These provide relatively similar values, considering the strong uncertainty associated with each κ_r measurement. The frequency ranges for these approaches are not the same, because $\kappa_{r\text{-AS}}$ involves

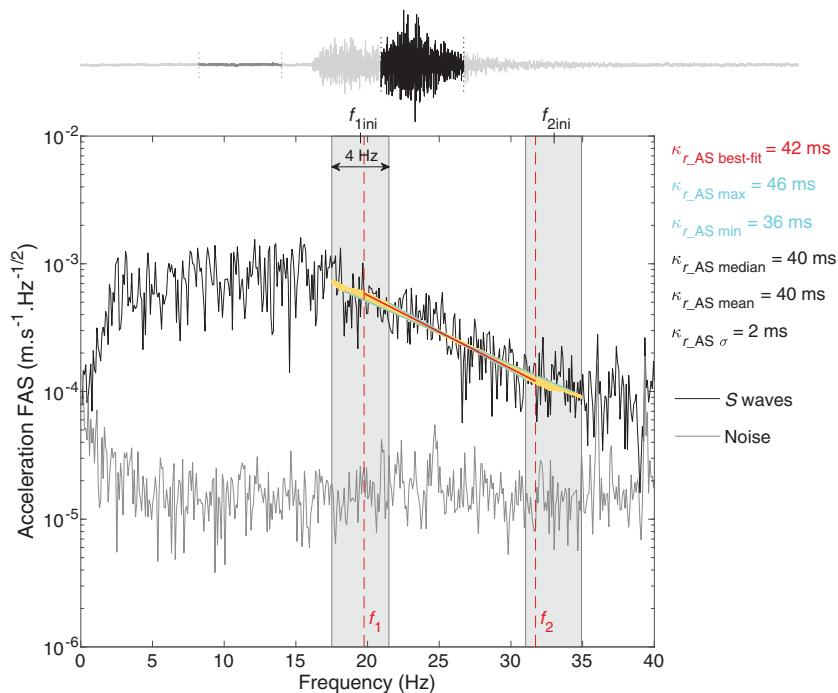


Figure 5. Example of κ_{r_AS} evaluation for site P2. (Top) East-west accelerogram with the corresponding windows taken for the noise and S waves. (Bottom) Horizontal mean component of the Fourier amplitude spectrum (FAS) density for the noise and for the S waves given with the procedure of evaluation of κ . The two initial frequencies picked by the operator (f_{1ini} , f_{2ini}) are used to define the two frequency windows (vertical gray bands) where the semiautomatic procedure is implemented. Between these two bounds, all of the combinations of the slope of linear regression are tested (yellow lines) to find the best in terms of the residuals of the regression (κ_{r_AS} best fit; red line) and the minimum and maximum slopes (κ_{r_AS} min, κ_{r_AS} max, blue lines).

higher frequencies than κ_{r_DS} , and the frequency window widths (Δf) are also slightly higher, in general, for κ_{r_AS} .

Figure 8 shows the comparison between the κ_0 evaluations for these acceleration and displacement approaches and provides a summary of the main features of the results. Here, the recordings at rock sites P1 and P2 are processed together to provide the maximum events, to estimate the statistics for each approach, and to derive a regional m_κ from both sites (Anderson and Humphrey, 1991; Ktenidou *et al.*, 2013). The first expected result is that the number of usable events is somewhat lower with the acceleration method than with the displacement method. Moreover, the event extraction methodology from the national catalogs that follows here imposes a lower limit on the exploitable magnitude range, which penalizes the displacement method. Indeed, local events of very small magnitude ($M < 1.5$) that are not listed in the catalogs are not processed, even though they are particularly suitable for this approach. In addition, the acceleration method benefits from the 10 years of pre-existing triggered instrumentation for site P2 because only the higher magnitude events were recorded. As shown in Figures 7 and 8, the measurement frequency range (characterized by the distribution of the central frequency $f_{mean} = 1/2(f_1 + f_2)$) is definitely higher for κ_{r_AS} than for κ_{r_DS} , and the measure-

ment bandwidth Δf is also a little higher for κ_{r_AS} . The event-to-event variability in the individual κ_r estimates, together with the associated uncertainties, is higher for the displacement approach, especially at large epicentral distances. This also leads to larger uncertainties in the estimation of κ_0 and m_κ for the displacement approach.

The discrepancy between κ_{r_AS} and κ_{r_DS} increases with increasing R_e (Fig. 8) due to the much lower m_κ slope for the acceleration approach ($m_{\kappa_DS} > 3m_{\kappa_AS}$). This large difference might explain why, compared with κ_{0_AS} , κ_{0_DS} is lower, whereas $\kappa_{0_DS} < 30$ km estimated from the nearest events is greater than $\kappa_{0_AS} < 30$ km. However, the dependence of κ_r on R_e is discussed later in terms of the Q -values obtained in previous studies in this region. Nevertheless, the κ_0 are very similar for both approaches, as close to 30 ms on average for the hard rock of the studied site. This is relatively high for sites with $V_{S30} \approx 2000$ m/s, in comparison with those commonly proposed in the literature based on V_{S30}/κ_0 correlations (Ktenidou *et al.*, 2014, 2015), although it still remains within the (large) uncertainties associated with such correlations. This is consistent with the $\kappa_{0_AS} = 26$ ms obtained by Douglas *et al.* (2010) for the

Alps. However, the study of Douglas *et al.* (2010) is not fully comparable with the observations of the present study, because they used mean κ_{0_AS} from many rock sites under different site conditions, which are not likely to have been all as hard as the present site.

Analysis of the Sensitivity and Robustness of κ to Various Parameters

Measurement Uncertainty $\Delta\kappa_r$

The data obtained from the acceleration and displacement approaches provide the opportunity to determine the sensitivity of the individual κ_r estimation uncertainties ($\Delta\kappa_r$) to various parameters where individual κ_r values are computed, such as the local magnitude (M_L), the epicentral distance (R_e), and the frequency window mean (f_{mean}) and width (Δf). As explained above (Fig. 5), this uncertainty corresponds to the variability of the spectral regression slope over all the considered frequency intervals ($\Delta\kappa_r = \kappa_{r_max} - \kappa_{r_min}$).

Figure 9 shows $\Delta\kappa_r$ as a function of M_L , R_e , f_{mean} , and Δf for the acceleration and displacement approaches. Although some trends can be seen between $\Delta\kappa_r$ and mainly M_L , f_{mean} , and Δf , the general trend differs greatly when considering $\Delta\kappa_{r_AS}$ and $\Delta\kappa_{r_DS}$. Moreover, a strong trade-

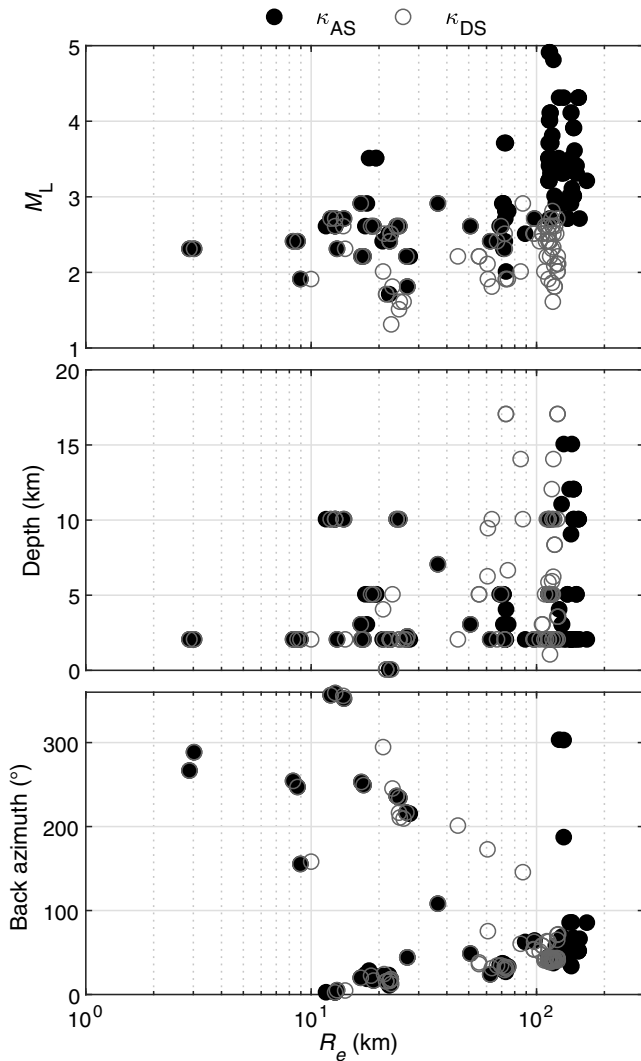


Figure 6. Comparisons of the dataset used for the κ_{AS} method (black filled circles) and the κ_{DS} method (gray circles), in terms of the magnitude (M_L), depth, and back azimuth, according to the epicentral distance (R_e).

off is suspected between M_L or f_{mean} and Δf . Indeed, when the magnitude is high, then f_c is low, and the SNR is often good up to high frequencies, which provides a wide frequency range to measure κ_{r_AS} (high Δf). In contrast, low f_c values constrain the evaluation of κ_{r_DS} to the low-frequency range, which restricts Δf . In the same way, an increase in f_{mean} for the acceleration approach indicates generally decreased Δf , whereas this is the opposite with κ_{DS} . These differences between the two approaches for the Δf trade-off with M_L and f_{mean} appear to explain the differences in the behaviors of these parameters with $\Delta\kappa_r$, whereby it is finally Δf that primarily controls the uncertainty on κ_r . However, the apparent dependence of $\Delta\kappa_r$ on Δf is probably increased by the choice of a constant width (± 2 Hz) for the investigated frequency band, which impacts more on a short window than a long one. Nevertheless, the minimum width of 10 Hz reduces this bias. After removing

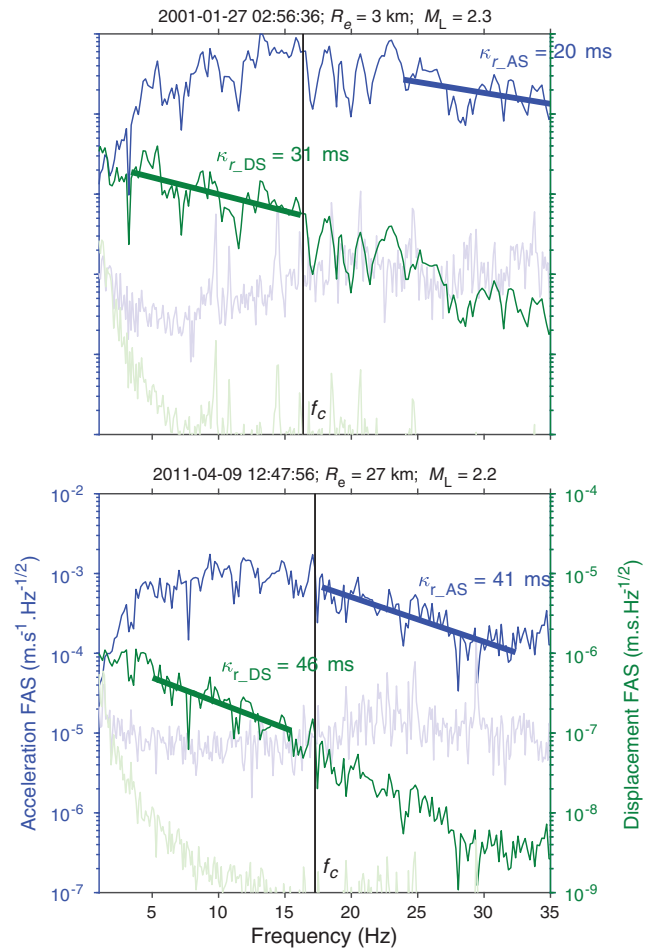


Figure 7. Comparisons of the individual κ_{r_AS} (blue) and κ_{r_DS} (green) estimations for two earthquakes at site P2. The vertical black line on each plot represents the picked corner frequency of the source (f_c).

the parts due to the trade-off between Δf and the M_L and f_{mean} trends, the data (not shown) are convincing in terms that the dependence of the κ_r uncertainty on M_L , R_e , and f_{mean} is negligible, because this can be almost totally explained by Δf . $\Delta\kappa_r$ actually exhibits exponential decay with increasing Δf . This sensitivity to Δf is likely to be associated with several physical factors (site amplification, frequency-dependent attenuation, and source effects on κ_r). These are discussed in the next sections.

Frequency Dependence of the Attenuation

As indicated in the [Introduction](#), κ is assumed to be related to the frequency-independent component of Q , thus ignoring the scattering component of the attenuation. When considering propagation in the crust only, equation (5) can be simplified into

$$Q_i = \frac{1}{V_S m_\kappa} \quad (8)$$

([Hough et al., 1988](#); [Ktenidou et al., 2015](#)), in which Q_i describes the intrinsic crustal attenuation only, and V_S is the

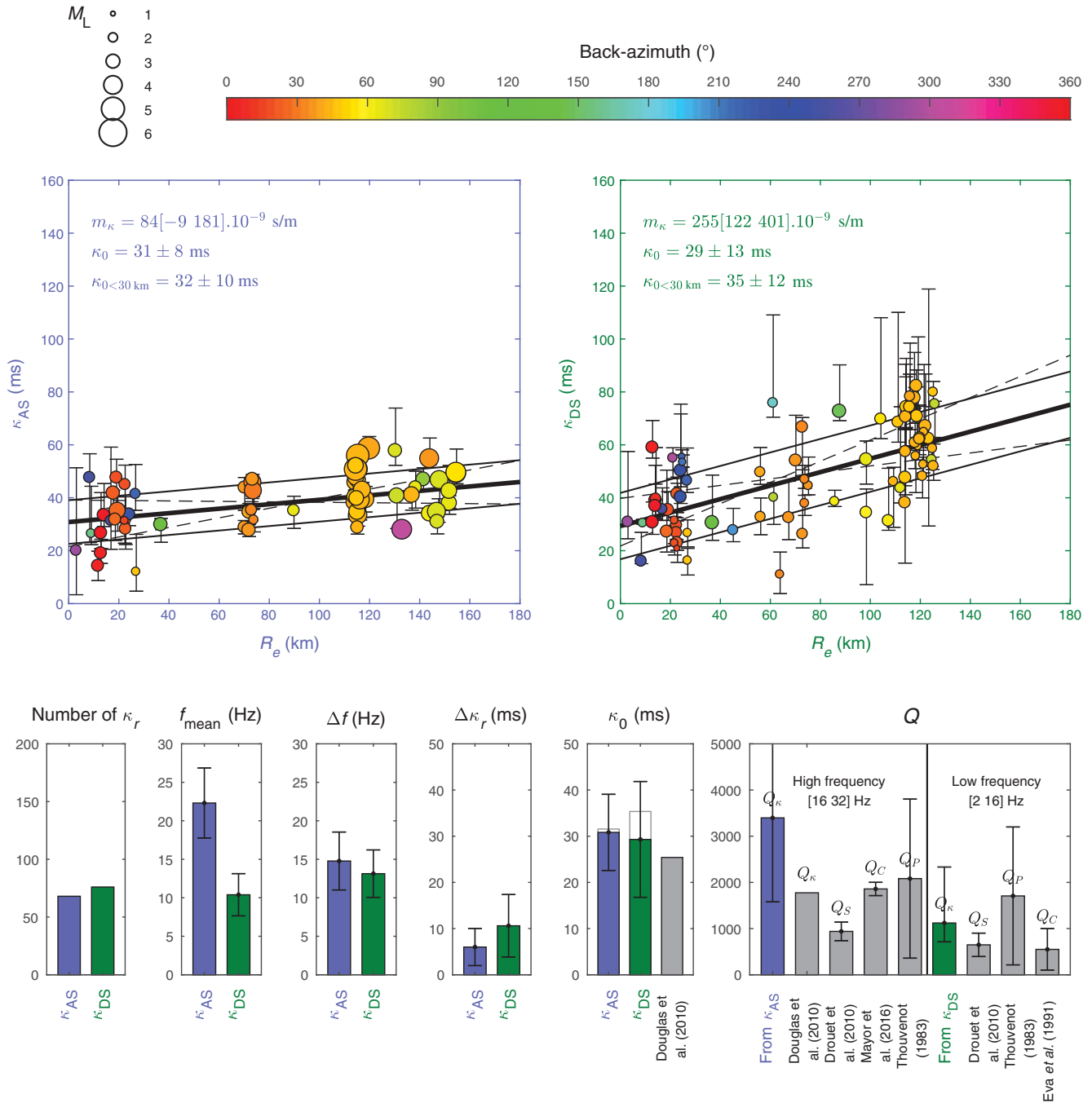


Figure 8. Comparisons between (top left, purple) κ_{AS} and (top right, green) κ_{DS} evaluations at the rock sites P1 and P2, taken together. (Top) κ_r represented with the uncertainties ($\Delta \kappa_r$) as a function of the epicentral distance (R_e). The linear regression (thick solid line) gives the slope (m_κ) for the distance-dependence model, with the associated uncertainties (dashed lines) and the zero intercept (κ_0) with its uncertainties (thin solid lines). The $\kappa_{0 < 30 \text{ km}}$ approximation as the mean of the κ_r for $R_e < 30 \text{ km}$ is given as well. (Bottom) Statistics (generally as means \pm one standard deviation) associated with each method: (left to right) the number of individual estimations of κ_r , central values (f_{mean}) and widths (Δf) of the frequency ranges used to determine κ_r , $\Delta \kappa_r$, κ_0 , and $\kappa_{0 < 30 \text{ km}}$ (gray), and finally the Q values deduced from κ_r and compared with those available in the literature for the Alps region.

mean shear-wave velocity in the crust. To avoid making any assumption in equation (8), this Q estimate from the m_κ values is referred to as Q_κ . Figure 8 includes comparisons between Q_κ and Q from previous studies in the Alps. For this, a shear-wave velocity of $V_S = 3500 \text{ m/s}$ was assumed, which is a standard value for the crust. The $m_{\kappa_{AS}}$ value of

Douglas *et al.* (2010) is also translated into the Q_κ value and compared with the other values of Q at high frequencies. Mayor *et al.* (2016) estimated a value of Q_C from the coda of between 16 and 32 Hz, whereas Eva *et al.* (1991) proposed a Q_C value between 2 and 16 Hz. Thouvenot (1983) proposed a $Q_P(f)$ model from P waves recorded during a few active

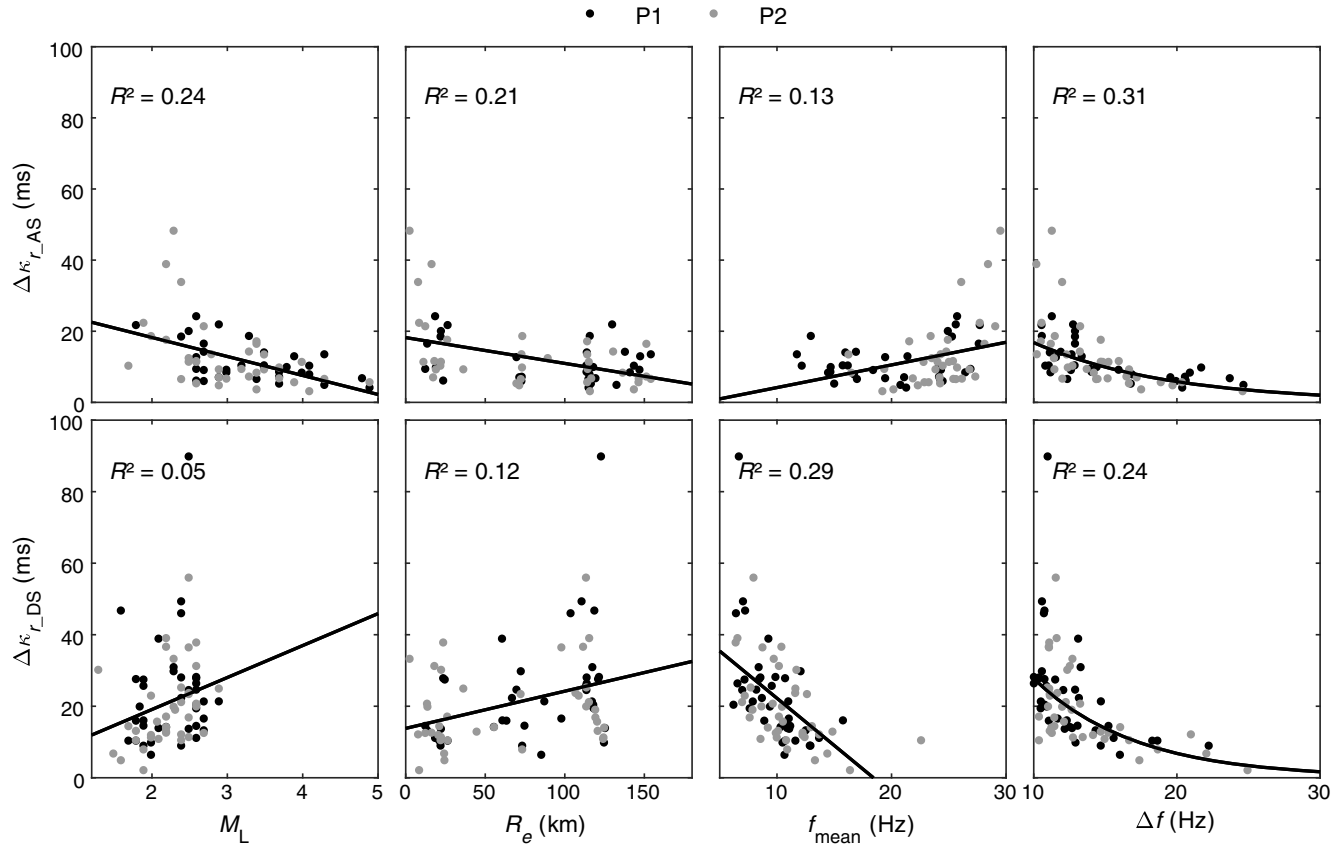


Figure 9. Evaluation of the dependence of the κ_r uncertainty ($\Delta\kappa_r$) on local magnitude (M_L), epicentral distance (R_e), frequency window mean (f_{mean}), and width (Δf) used to assess κ_r , shown for the (top) κ_{AS} and (bottom) κ_{DS} approaches. For each plot, the linear trend is represented with its corresponding determination coefficient (R^2). For Δf , an exponential model is preferred to the linear trend. Black and gray circles represent the results for sites P1 and P2, respectively.

deep sounding experiments, and in a different way, [Drouet et al. \(2010\)](#) also established a $Q_S(f)$ model from a generalized inversion-technique scheme on the S -wave phase of earthquake recordings. Here, values at high (16–32 Hz) and low (2–16 Hz) frequencies are calculated from these two $Q(f)$ models. The high-frequency Q deduced from these models are compared to the $m_{\kappa_{\text{AS}}}$ evaluations, whereas the low-frequency Q are compared to those deduced from the present $m_{\kappa_{\text{DS}}}$ value.

The values from previous studies show large scatter, which is not surprising, because they were evaluated from different techniques in different phases of the signal (i.e., P waves, S waves, and coda waves) and for different locations in the Alps. Moreover, Q_c is primarily controlled by the absorption (Q_i ; [Aki and Chouet, 1975](#)), whereas Q_P and Q_S provide access to the full attenuation Q_{ef} that also includes the scattering ([Campbell, 2009](#)). In [Figure 8](#), the Q_P estimates present higher values, especially at low frequencies, whereas the Q_S and Q_c estimates are comparable. The evaluation of Q_κ at lower frequencies from $m_{\kappa_{\text{DS}}}$ is in good agreement with previous studies because it is within most of the variability ranges. At high frequencies, the very small $m_{\kappa_{\text{AS}}}$ values lead to Q -values much larger than those reported in

the literature. This inconsistency with previous studies can be explained again by the large differences between each approach. Even considering [Douglas et al. \(2010\)](#), who followed the same κ_{AS} procedure, this is not fully comparable, because they used many stations from many locations in the Alps to determine $m_{\kappa_{\text{AS}}}$.

Limited impact on the uncertainty is expected for the source and path components, because all of the events were crustal low-to-moderate magnitude earthquakes that are mainly from the same narrow azimuthal range ([Fig. 6](#)). Nevertheless, a strong threefold discrepancy appears between $m_{\kappa_{\text{AS}}}$ and $m_{\kappa_{\text{DS}}}$ ([Fig. 8](#)). A possible explanation for this is that $m_{\kappa_{\text{AS}}}$ refers to a higher frequency range than $m_{\kappa_{\text{DS}}}$. This difference in the frequency range in which m_κ is measured might explain the discrepancy between the slopes obtained from each of these methods because Q is widely accepted to increase as the frequency increases. However, the difference between the previous estimates of high- and low-frequency Q is significantly lower than the difference inferred here from the m_κ data. Thus, the frequency dependence of Q might partly explain the discrepancy observed between $m_{\kappa_{\text{AS}}}$ and $m_{\kappa_{\text{DS}}}$, but probably not all.

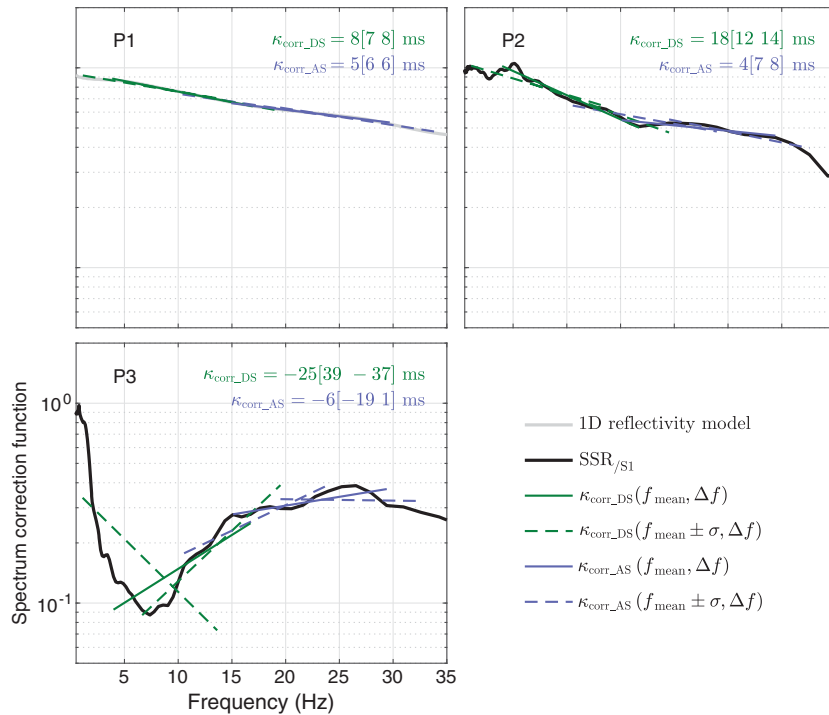


Figure 10. Perturbation of κ induced by site amplification for sites P1–P3. The spectral correction functions are estimated as the inverse of the site transfer functions. At sites P2 and P3, the empirical site transfer functions were computed from the SSR (black) according to the reference site P1. At site P1, the theoretical site transfer function was computed through the 1D reflectivity model approach, based on the *in situ* velocity profile. The linear trend was computed from the transfer function in the frequency range defined by $(f_{\text{mean}}, \Delta f)$ and $(f_{\text{mean}} \pm \sigma, \Delta f)$ for κ_{AS} (purple) and κ_{DS} (green), in which Δf is the mean width, f_{mean} is the mean, and σ is the standard deviation of the central frequency of the frequency windows used to determine κ_r . The κ values deduced from these linear trends are also indicated.

Site Amplification Dependence of κ

According to most studies, κ_0 is linked to the *S*-wave attenuation due to the geological structures beneath the site. In GMPEs or host-to-target adjustment techniques, κ_0 reflects only the attenuation, while the amplification is generally taken into account mainly through V_{S30} . However, attenuation and amplification impact the same frequency range and are difficult to separate in practice. κ_0 measurements without due consideration to site amplification may thus be significantly biased in an unpredictable way: sedimentary basins generally exhibit large amplifications that are strongly frequency dependent over a wide frequency range (Fig. 4), whereas the presence of a weathered zone on rock sites can also produce high-frequency amplification. These site effects modify the FAS shapes and can thus bias the κ_r evaluation. The site amplification is expected to modify κ_0 mainly and m_κ only slightly, because every κ_r is biased approximately in the same manner, as long as it is evaluated for a similar frequency range. Various studies have made the assumption that reliable evaluation of κ_r is possible, as long as the analysis frequency windows are chosen out of the fundamental resonance frequency range

of the site (f_0) and in a sufficiently wide frequency range (Hough *et al.*, 1999; Parolai and Bindi, 2004; Ktenidou *et al.*, 2013). However, this assumption is doubtful when the site amplification is complex (2D and 3D) and/or broadband, and it is difficult to respect this in a low-to-moderate seismicity context, in which the spectral windows used to evaluate κ_{r_AS} are generally narrower compared to those available in higher seismicity areas. For instance, sites P3 and P4 show broadband amplifications (Fig. 4) that might have different impacts on κ_r due to the difference in the spectral shape, even if these sites are located near to each other in the same valley. Another approach consists of evaluation of κ_r from recordings that have been initially deconvolved (corrected) from the site transfer function. Recently, taking into account only the amplification, deconvolution by the theoretical 1D transfer function was tested but did not provide convincing results (Van Houtte *et al.*, 2011; Ktenidou *et al.*, 2013). The main difficulties of such an approach are the availability of a well-known velocity profile for theoretical computation, the validity of the 1D approximation, and the potential introduction of some uncertainty associated with the transfer function on κ . In contrast, when using empirical approaches (e.g., SSR and generalized inversion technique), the difficulty is to separate the amplification and the attenuation.

Figure 10 is designed to show the correction function that is needed to correct the FAS before computing κ_r values, to account for site effects. For sites P2 and P3, these correction functions are given using the inverse of the relative site transfer functions estimated from the SSR approach at the sites, with site P1 taken as reference (Fig. 10, black curves). For site P1, the correction function is the inverse of the theoretical transfer function that is computed from the 1D reflectivity model (Kennett, 1974; Fig. 10, gray curve), based on the *in situ* velocity profile available at this site. To understand how the site response influences the κ_r evaluation, the linear trends of the correction function are shown in Figure 10. The slopes of these trends quantify the corrections that will modify the κ_r evaluations, which are denoted as $\kappa_{\text{corr_AS}}$ and $\kappa_{\text{corr_DS}}$. The slopes are computed on the site correction functions for the frequency windows defined by the mean of Δf and f_{mean} used for the κ_{r_AS} and κ_{r_DS} determinations (Fig. 10, blue and green solid lines, respectively). The means of $f_{\text{mean}} \pm$ standard deviation (σ) are also given, to infer the frequency dependence induced on κ_r by the site effects (Fig. 10, blue and green dashed lines).

From the correction inferred from the theoretical site amplification for site P1, it can be seen that due to the shallow weathered zone, the velocity gradient within the first meters in depth also induces amplification that can bias the measures of κ (+5 to +8 ms), even if this is a hard-rock site. Site P2 is also a hard-rock site, and it is very similar to site P1, and thus small κ differences are expected between these two sites. The SSR transfer function between sites P2 and P1 shows two main linear trends with a different bias for κ_{r_AS} (+4 to +8 ms) and κ_{r_DS} (+12 to +18 ms) but do not increase the frequency variability by much. For the soil site P3, the strong relative amplification below 15 Hz induces very variable and important modifications to κ_{r_DS} that depend on the frequency window (+39 to -37 ms). At higher frequencies, the transfer function is flatter, which leads to κ_{r_AS} evaluations that are less dependent on the site responses.

The real influence of the site amplification on κ is shown in Figure 11, through a comparison between sites P1, P2, and P3. To understand how the site effects interact with κ , κ_r evaluations that are made from the FAS deconvolved by the theoretical (for site P1) and empirical (for sites P2, P3) site transfer functions are also shown in Figure 11. It should be noted here that the whole processing procedure, which included the frequency bound (f_{1ini} , f_{2ini}) picking, was performed after the deconvolution. This is important, because the site amplification can also change the apparent linearity of the FAS and lead operators to select mistaken frequency bounds for κ_r evaluation. In Figure 11, the κ_{AS} results are given on the left, with the κ_{DS} results on the right. For each panel in Figure 11, the individual κ_r measurements are represented according to the epicentral distance, for which the diameters of the symbols are proportional to the magnitudes, and their color indicates the back azimuth of the corresponding event.

First, for the κ_{AS} method, the results at the two rock sites (sites P1 and P2) show similarities in terms of both κ_{0_AS} and m_{κ_AS} , as the discrepancy is within the variability of the measurements. This is consistent with the spatial and geological proximity of these two sites. However, we observed some significant differences for a few of the individual κ_{r_AS} evaluations between these two sites. Indeed, modification of the FAS by the site effect can lead to higher frequency evaluations for site P2 than site P1, due to the slope change in the SSR at around 17 Hz (Fig. 10). The displacement method shows greater discrepancy between these two sites. The slope m_{κ_DS} for site P1 is almost twice that of site P2, and the site component κ_{0_DS} is a little lower for site P1 than site P2, although this difference can be easily explained by the differences in the slope. Indeed, the slope-independent $\kappa_{0_DS<30\text{ km}}$ is similar for sites P1 and P2. Moreover, as expected, $\kappa_{0_DS<30\text{ km}}$ is higher at site P1 than site P2, contrary to κ_{0_DS} . Differences in the slopes between sites P1 and P2 cannot be explained physically, because the regional attenuation must be the same for all of the sites and is expected to be proportional to the regional Q_i (Ktenidou *et al.*, 2015). This can be attributed to the large scatter on the individual

κ_{r_DS} , to the lack of measured points at short epicentral distances for site P1 to constrain the slope, and to the differences in the input dataset. At stiff-soil site P3, κ_{0_AS} is very similar to the values obtained for the rock sites. At first glance, a higher value of κ_{0_AS} might be expected for this stiff soil of site P3, because such sites are classically more attenuating than rock sites. However, the influence on κ_{0_AS} of the shallow stiff-soil basin might be limited, because this parameter is assumed to infer attenuation down to deep geological structures (Ktenidou *et al.*, 2015).

The influence of site transfer function deconvolution on κ_0 might be roughly predicted by the κ_{corr_AS} and κ_{corr_DS} obtained from the slopes of the site correction function (Fig. 10). Deconvolution of the hard-rock sites P1 and P2 provides κ_{0_AS} and κ_{0_DS} results that are close to those predicted by the site correction function given in Figure 10. As predicted, the deconvolved κ_{0_AS} are only slightly changed as they are within the variability band of the raw estimation. For site P3, the κ_{0_AS} modification (-1 ms) does not agree well with the prediction (-6 ms). Moreover, the scatter in κ_{r_AS} and κ_{r_DS} is slightly reduced, and the number of individual κ_{r_DS} available increases after the deconvolution. These observations suggest that the site effects disturb the linearity of the spectrum decay for site P3, which led the operator to remove some events or to improperly select the initial frequency bound for other events. At sites P2 and P3, the deconvolution was computed from the SSR transfer function relative to site P1. This correction should provide κ results at the site that are very close to those obtained at the reference site because the site is thus placed according to both the amplification and attenuation conditions of the reference. Then, strong similarities are expected between the deconvolved sites P2 and P3, and site P1. This convergence toward site P1 is not realized in Figure 11, especially for κ_{DS} . These observations probably do not agree because of differences in the datasets used for the different sites, and because of the introduction of uncertainties by the SSR deconvolution. We do not expect such differences to be due to differences in the deep structure, as suggested by Ktenidou *et al.* (2015), because the deep structure (i.e., beyond, at most, 100 m in depth) should be the same for all sites. The impact of site and of crustal amplification on κ_0 is estimated through deconvolution of the 1D theoretical transfer function at site P1, similar to what was done by Van Houtte *et al.* (2011) and Ktenidou *et al.* (2013). Figure 11 shows that κ_{0_AS} and κ_{0_DS} increased notably after the deconvolution, mainly due to the site amplification rather than to the crustal amplification, because the transfer function is widely controlled by the former. Thus, the site amplification cannot be neglected, even for hard-rock sites.

To conclude this section, it can be seen that the site-effect influence can be high and variable, depending on the frequency band. Moreover, in agreement with recent studies (Van Houtte *et al.*, 2014; Edwards *et al.*, 2015; Laurendeau *et al.*, 2017), the site amplification can explain a part of the observed κ variability, because it is frequency dependent, and

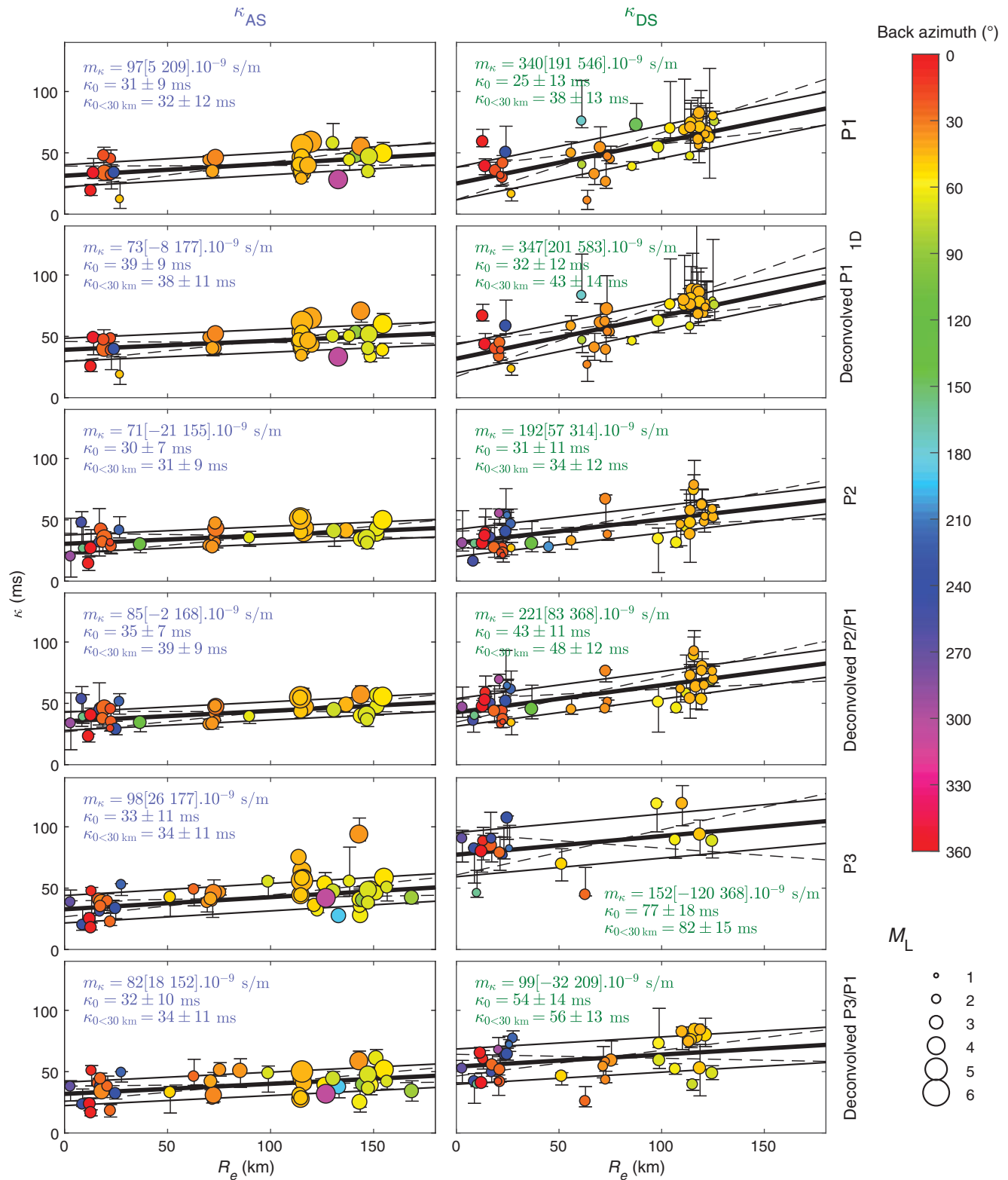


Figure 11. Estimation of κ_r , κ_0 , $\kappa_{0<30\text{ km}}$, and m_κ (slope) from the (left) κ_{AS} and (right) κ_{DS} approaches for the two hard-rock sites (P1 and P2) and the stiff-soil site (P3). At sites P2 and P3, the results are obtained after deconvolution of the recordings by the relative transfer functions estimated by SSR, with site P1 as reference. For site P1, the deconvolution is realized from the theoretical 1D reflectivity model site amplification function. κ_0 and m_κ are estimated from linear regression, in which each κ_r is weighted by the inverse of its variability ($\Delta\kappa_r$).

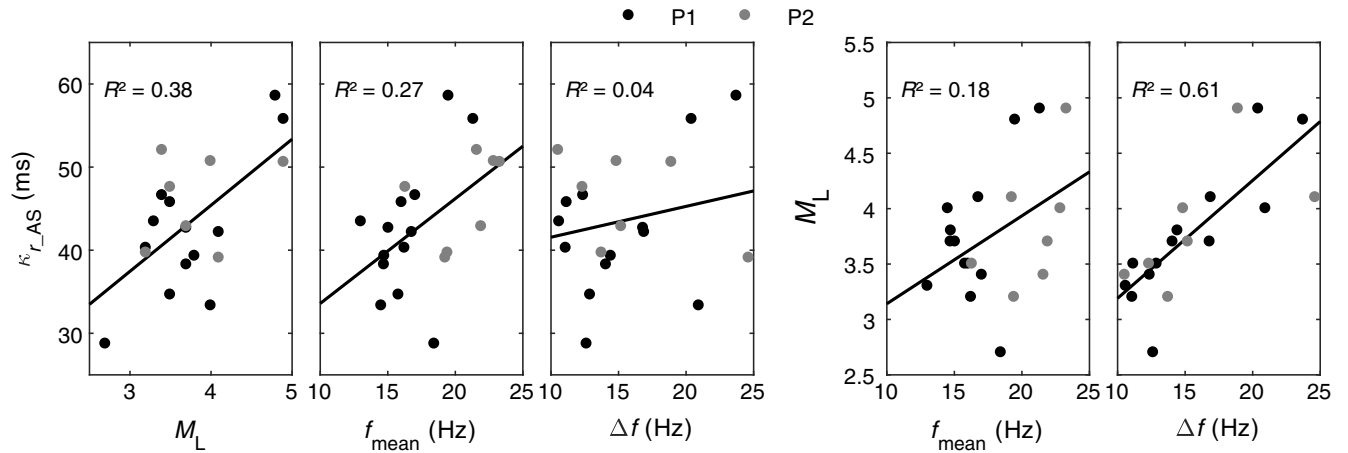


Figure 12. Evaluation of the source dependence of κ from the correlation between κ_{r_AS} and the local magnitude (M_L) for earthquakes approximately in the same position (a cluster of events located at ~ 120 km epicentral distance and azimuthal direction N50°E). (Left) The potential trade-off between M_L and the frequency windows chosen to measure κ_{r_AS} is illustrated by the correlation between M_L and the central frequency (f_{mean}) and width (Δf) of the frequency window. (Right) The influence of the frequency window on κ is illustrated by the correlation of κ_{r_AS} with f_{mean} and Δf . Black and gray circles define κ_{r_AS} from sites P1 and P2, respectively; the linear trend is represented by the corresponding determination coefficient (R^2).

each individual κ_r is measured for different frequency windows. Thus, κ should be considered carefully, as a site amplification component cannot be excluded even for rock sites, especially for low-seismicity context when κ_r are estimated from limited spectral windows.

Source Dependence of κ

The assumption of a negligible source contribution for κ relies on the validity of the ω^{-2} source model (Brune, 1970). Any variation from this model or any bad consideration of the f_c criteria can impact upon the measurement of κ . To evaluate the validity of this assumption, the two recorded seismic sequences of Jausiers are considered. The Jausiers cluster of points is shown in Figures 6 and 8, close to the 120-km epicentral distance and at \sim N50°E azimuth. All of the events are collocated, so the records share at least the same site and path components.

Figure 12 shows the linear trend for the clusters between the κ_{r_AS} individual values estimated at sites P1 (black filled circles) and P2 (gray filled circles), and the local magnitudes. The associated coefficient of determination (R^2) is also shown. Although there are not enough data points to form any conclusions here, in Figures 8 and 12, higher magnitudes appear to correspond to higher κ_{r_AS} . For κ_{r_DS} , this trend cannot be seen in Figure 8 and is not represented in Figure 12, due to the too narrow range of the magnitudes that is available with the displacement method. An initial possible explanation is that κ is dependent on the magnitude, in agreement with some previous studies that have argued for its source dependence (Papageorgiou and Aki, 1983; Aki, 1987; Papageorgiou, 1988, 2003; Gariel and Campillo, 1989; Wen and Chen, 2012). A second explanation is that the decrease in κ_{r_AS} is due to the shortening of Δf for decreasing magnitudes (Fig. 12), which makes its measurement less

robust, as observed through the increase in $\Delta\kappa_{r_AS}$ for decreasing Δf (Fig. 9). Indeed, the κ_{r_AS} estimate at low magnitudes can be more sensitive to the bad consideration of the f_c criterion. Indeed, because of the source spectrum shape in acceleration that increases up to f_c and is then flat, if f_1 is taken below f_c , this would result in an underestimation of κ_{r_AS} (Boore and Campbell, 2017; Ktenidou *et al.*, 2017). Moreover, it should be noted that the source model is not bilinear, but has a smooth transition around f_c that is described by the gamma parameter. This means that f_1 should be taken a few hertz above f_c to avoid any influence of the sloped part of the source spectrum. However, in practice, the limited bandwidth that is available to measure κ_{r_AS} provides such a precaution, especially for low-magnitude events. In addition, f_c is difficult to determine due to site effects that modify the spectrum and then potentially hide the correct value. For the displacement approach, if f_2 exceeds f_c , this should result in an increase in κ_{r_DS} . The stress drop of small-magnitude events is very uncertain, which makes this latter approach very sensitive to f_c . This phenomenological difference between the two approaches might explain, at least in part, why κ_{r_DS} generally exceeds κ_{r_AS} (Ktenidou *et al.*, 2017).

However, the possible influence of the frequency windows for κ_{r_AS} is not clear in Figure 12. It appears that lower f_{mean} and narrower Δf correspond to lower κ_{r_AS} , although the correlations are not very good, especially for Δf . The linear regression shows low correlation between f_{mean} and κ_{r_AS} ($R^2 = 0.27$), whereas no correlation is seen for Δf ($R^2 = 0.04$). The investigation of the trade-off between f_{mean} and Δf with the magnitude is given on the right in Figure 12. The correlation between the magnitude and f_{mean} is not clear ($R^2 = 0.18$), whereas that with Δf is evident ($R^2 = 0.61$). This latter parameter is not correlated with

κ_{r_AS} , so the possible bias of the lower magnitudes due to the associated frequency windows appears not to explain very well the apparent magnitude dependence of κ_{r_AS} . Only a limited part of the influence of the trade-off between the magnitude and the frequency range for which κ_{r_AS} is evaluated can be explained, and this is highly uncertain.

No influence of the depth was found, because this parameter was only slightly variable between the events, and because this information was extracted from the national bulletin and was thus affected by relatively large uncertainty. Moreover, this result is in agreement with [Edwards et al. \(2011\)](#), who showed that the linear trend between attenuation and distance indicates limited depth dependence for κ_r .

To conclude this section, among the different explored source parameters, the best correlation with κ_r appears to be for the magnitude, and this appears to be explained by the source dependence, rather than by bias on the lower magnitudes due to the overlap of the frequency window with f_c . However, the correlation remains rough, and the uncertainties on κ_{r_AS} and the local magnitude estimations are too large to be conclusive on this point.

Discussion

The site component of κ , κ_0 , is widely used in hazard seismology to constrain the high-frequency spectral shape in stochastic simulations, in some GMPEs, and for host-to-target adjustment. The underlying interpretation is that κ_0 represents the S -wave attenuation by the geological structure beneath the site. However, because the physics of κ is not fully captured, it is important to discuss to what extent the κ_0 estimates may be biased by the limitations of data available in low-seismicity areas and the associated origins of the large variability observed in κ_r measurements. These two issues are discussed separately, even though some physical phenomena may affect simultaneously the bias and scatter of κ_r measurements, before a final discussion on the validity of the κ_{DS} approach, because it seems well suited to low-to-moderate seismic areas.

Reliability of the κ_0 Measurements

In GMPEs or host-to-target adjustment, κ_0 only reflects the frequency-independent attenuation. However, the underlying physics are still debated. As mentioned before, the site amplification, the frequency dependence of attenuation, and the earthquake source might bias κ_0 estimates by systematically moving up or down individual κ_r measurements.

The effects of the site amplification have been reported in several instrumental and simulation studies. [Ktenidou and Abrahamson \(2016\)](#) observed negative apparent κ_0 on many hard-rock sites, which they attributed to biasing effects of site amplification. It has been often considered that κ_r may be reliably estimated when the frequency interval over which the spectral decay is measured is broad enough and does not include the fundamental resonance frequency of the site (f_0 ;

[Hough et al., 1999](#); [Parolai and Bindi, 2004](#); [Ktenidou et al., 2013](#)). This assumption was supported by simple 1D simulations ([Parolai and Bind, 2004](#)) and is easy to implement in practice because f_0 can be easily determined through the horizontal-to-vertical spectral ratio approach computed either from microtremors (e.g., [Nakamura, 1989](#); [Kudo, 1995](#)) or from earthquake recordings (e.g., [Lermo and Chávez-García, 1993](#)). As mentioned earlier, there are many cases, however, where complex broadband site effects hamper κ_0 measurements. We show that even for hard-rock sites, high-frequency amplification systematically biases κ_r in a similar manner for a given approach (Fig. 10), resulting in a significant impact on the accuracy of κ_0 (by about 25%–30%), with only weak changes for the regression slope with epicentral distance m_κ (Fig. 11). For soil sites, the site amplification influence is large, and almost impossible to correct, when f_0 is included in the analysis frequency windows for both κ_0 and m_κ (κ_{DS} at site P3, in Figs. 10 and 11), and it is prejudicial otherwise (κ_{AS} at site P3, in Figs. 10 and 11).

In a similar way, the frequency dependence of the attenuation may impact the value of κ_0 , at least through the measurement frequency interval. [Boore and Campbell \(2017\)](#) provided an illustrative example of the large variability of κ_0 obtained for the same site (Pinyon Flat Observatory, California) with different approaches. The frequency-independence assumption was formulated during the introduction of κ by [Anderson and Hough \(1984\)](#) and later by [Hough and Anderson \(1988\)](#), with reference to several previous studies ([Warren, 1972](#); [Rovelli, 1982](#); [Anderson, 1986](#)). [Anderson et al. \(1996\)](#) also reported a negligible influence of Q_{sc} from numerical simulation for velocity and Q profiles with pluri-hectometer thick layers. However, the frequency dependence of Q_{sc} and even sometime of Q_i was actually shown by various studies (e.g., [Aki and Chouet, 1975](#); [Calvet et al., 2013](#); [Mayor et al., 2016](#)). When introducing their model (equation 5), [Hough and Anderson \(1988\)](#) already indicated that even a slight frequency dependence of Q_{ef} will yield a smaller value of κ . [Edwards et al. \(2015\)](#) also recently supported the frequency-dependence interpretation through a comparison of κ results from different approaches involving different frequency bands. They also observed that the high-frequency spectral decay was generally not well explained by the linear κ_r attenuation model (equation 1), but rather by a curved or bilinear model. [Parolai et al. \(2015\)](#) showed a nonnegligible role of scattering attenuation from numerical simulations, especially for small levels of intrinsic attenuation. They proposed a nonlinear model for the high-frequency decay due to the introduction of scattering when the FAS are determined from several-second-width time windows in the S waves. [Ktenidou et al. \(2015\)](#) attributed the discrepancy between borehole and surface κ_0 measurements to the scattering, which was recently confirmed by [Pilz and Fäh \(2017\)](#) showing that the scattering contribution to κ_0 should not be neglected. In the present study, we observe a strong three-fold discrepancy between m_{κ_AS} and m_{κ_DS} (Fig. 8) that

might be explained at least partly by the difference in the frequency range between each definition of κ . The impact of the frequency dependence is more difficult to assess on κ_0 , but as the attenuation decreases with increasing frequency, it might reduce κ_0 , as predicted by [Hough and Anderson \(1988\)](#). Moreover, when approximating the distance-dependence model through the linear assumption, any variation in m_κ will result in a variation in κ_0 . It is thus essential to compare the κ_0 values with the average κ_r values for the closest events (e.g., $\kappa_{0<30\text{ km}}$).

Finally, various studies have argued for source dependence of κ since it was first defined ([Papageorgiou and Aki, 1983](#); [Aki, 1987](#); [Papageorgiou, 1988, 2003](#); [Gariel and Campillo, 1989](#); [Wen and Chen, 2012](#)). Although the site interpretation is at present commonly accepted for the distance independent part of κ , source-induced biases due to deviations from the ω^{-2} model or misapplication of the f_c criteria are possible. Seismic clusters are particularly suitable to study the source dependence, because κ_r measurements of these events only differ by their source component. In the present study, κ_{r_AS} values from the Jausiers cluster show a trend for decreasing with decreasing magnitudes. However, no conclusive interpretation is possible for the role of the source on κ , due to the scarcity of the data.

To sum up, the accuracy of κ_0 in low-to-moderate seismicity areas appears to be primarily controlled by the site amplification, especially for soil sites, and then by the approximation made with the frequency and source independence assumption. One must note, however, that the last two effects on κ_0 are difficult to quantify and might be stronger than expected. Nevertheless, in this study we found a robust κ_0 estimate of 30 ms with both a κ_{AS} and κ_{DS} for the hard-rock sites that is consistent with the high attenuation indicated for the Provence region ([Mayor et al., 2016](#)) and with the κ_0 obtained by [Douglas et al. \(2010\)](#) for rock sites in the Alps. Moreover, even if this high κ_0 is in the upper part of the very scattered κ_0/V_{S30} correlation, this is in agreement with recent studies that indicate higher κ_0 values for hard-rock sites than was initially suggested ([Ktenidou et al., 2015](#), [Ktenidou and Abrahamson, 2016](#), [Boore and Campbell, 2017](#), [Laurendeau et al., 2017](#)).

Variability of κ_r Measurements

Most studies reporting κ measurements indicate strong scatter when the κ_r values are represented according to the epicentral distance and sometimes an important variability in individual evaluation of κ_r themselves. Both the frequency dependence of the attenuation itself and that introduced by the site amplification can increase the frequency dependence of κ_r . This can explain a part of the variability between κ_r values, because they are evaluated over a variable frequency window. [Edwards et al. \(2015\)](#) showed that site amplification can have a strong influence on κ_{r_AS} , which depends on the frequency window considered, even for a hard-rock site. [Van Houtte et al. \(2014\)](#) observed an important variability of

κ_{r_AS} with the component orientation, and they attributed this to site effects. In the present study, we observe that when f_0 is included in the analysis frequency range, the site amplification greatly increases the frequency dependence of κ_r (κ_{DS} at site P3 in [Fig. 10](#)) and only slightly increases the scatter between the κ_r values (κ_{r_DS} at site P3 in [Fig. 11](#)). In the same way, the implicit approximation of a lateral homogeneity for the regional Q_{ef} included in the distance-dependence model (equation 3) is certainly not exact. However, no obvious influence of the back azimuth of the source is observed on κ_r here ([Figs. 8 and 11](#)), although it is not easy to separate it from the distance dependence. In the present study, we also evaluate the individual uncertainty of each κ_r ($\Delta\kappa_r$) through the variability of the spectral decay slope over varying frequency intervals. $\Delta\kappa_r$ is found to be primarily controlled by the width of this frequency interval (Δf). Small-scale variations in the FAS are thus very likely to perturb κ_r measurements for short Δf .

The effects of the source can be important, as highlighted through the high κ_{r_AS} scatter that was sometimes observed between events that belonged to the same cluster ([Kilb et al., 2012](#); [Ktenidou et al., 2013](#)). [Kilb et al. \(2012\)](#) attributed this to the variability of the near-source properties and the f_c values. In the present case, the former interpretation cannot be supported, because the magnitudes are small and the clusters are far enough apart to avoid near-field effects. For a subset of the Jausiers cluster events used in [Figure 12](#), [Figure 13](#) shows the influence of using variable ([Fig. 13, top](#)) or constant ([Fig. 13, bottom](#)) frequency windows over which κ_{r_AS} are evaluated. Using a constant frequency window for every event of this cluster, in which the back azimuth varies by less than 8° and the epicentral distance by less than 5%, should greatly reduce the scatter in the κ_{r_AS} values because almost no difference is expected between the κ_{r_AS} values for the site, the path, and the frequency dependence. Surprisingly, even if no clear correlation can be found between κ_{r_AS} and the magnitude, the strong scatter on the κ_{r_AS} values (30–60 ms) observed indifferently with variable or constant frequency windows appears to be an unambiguous link to the source for this hard-rock site. The constant frequency window that can be used for every κ_{r_AS} is relatively narrow ($\Delta f = 10$ Hz), which led to an increase in $\Delta\kappa_{r_AS}$ compared to that obtained with wider and more variable windows. However, the influence of Δf might not be preponderant here and cannot explain the strong scatter observed between the κ_{r_AS} values. Moreover, this is more likely due to variable deviations from the ω^{-2} model than to be linked to incorrect consideration of the f_c criteria. This means that the dominance of the source on the variability between κ_{r_AS} values is probably not specific to this study or to low-seismicity areas.

The κ_{DS} Approach

As discussed above, the evaluation of κ is variable and sometimes unreliable. This is particularly true when various

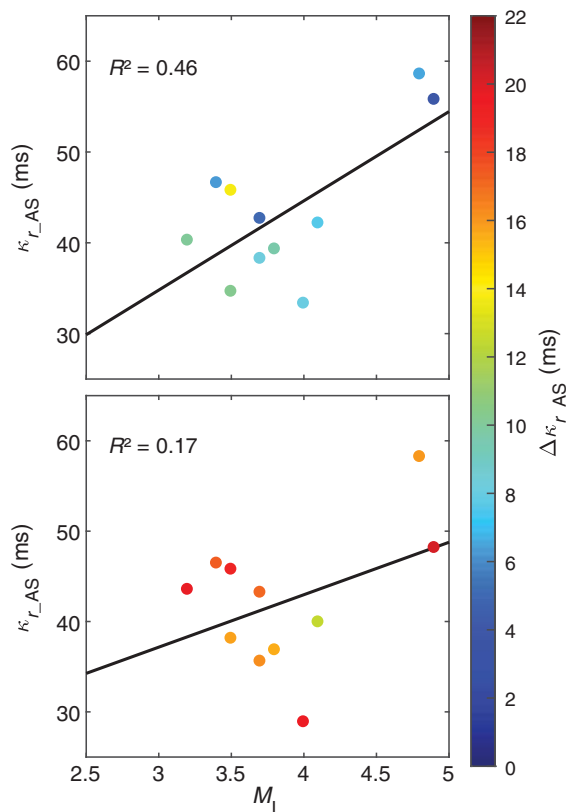


Figure 13. Evaluation at site P1 of the source dependence of κ_{r_AS} for a subset of the events from the Jausier cluster used in Figure 12. (Top) Each κ_{r_AS} value is estimated on the wider frequency window available. (Bottom) Same events, but with the κ_{r_AS} values calculated over the constant frequency window of 11.3–21.3 Hz. The color scale shows the variability associate with each κ_{r_AS} evaluation ($\Delta\kappa_{r_AS}$).

approaches are used to measure κ and in low-seismicity areas where the values of κ_r are evaluated over narrower and more variable frequency windows. Nevertheless, in such a context, all possible approaches have to be tested to improve the current practice, which consists of the deduction of κ_0 from the very uncertain κ_0/V_{S30} correlation (Kottke, 2017). The Biasi and Smith (2001) approach is very promising, because it is adapted to low-magnitude events that are generally the only events that can be recorded in low-seismicity areas over a reasonably short period of time. Moreover, the flatness of the displacement source spectrum below f_c is better understood than the ω^{-2} fall-off above f_c . This will lead to a potentially stronger influence of the source for κ_{AS} than for κ_{DS} . However, this presumed stronger robustness of κ_{DS} with respect to source spectral shape has not been observed in our results: κ_{r_DS} and κ_{r_AS} exhibit a comparable scatter (Figs. 8 and 11). Actually, κ_{DS} is likely to be more sensitive to the site amplification than κ_{AS} for soil sites, because it is evaluated in the 3–15 Hz frequency range that definitely overlaps with site resonance frequencies. For rock sites, the amplification is lower and is often at higher frequencies due to the very superficial velocity contrast that is generally induced by

the weathered zone. Moreover, the crustal amplification correction realized from the generic hard-rock profile has value basically for the κ_{DS} frequency range. Instead, at higher frequencies, the small-scale information of the velocity profile is generally unknown, which prevents the correction of the site amplification for κ_{AS} (Ktenidou and Abrahamson, 2016).

The use of velocimeters is strongly recommended for κ_{DS} because the accelerometers present a much lower sensitivity at low frequencies (<15 Hz; Fig. 3). In the present study, we used seismicity catalogs that did not include events for magnitudes below ~ 1.5 . These events are the most suitable for the κ_{DS} approach because they allowed very high f_c (15–50 Hz, depending on the stress drop). Thus, the κ_{DS} approach can be improved by detection and use of very small and generally local earthquakes from continuous recordings realized at the study site (although this was not done here), especially if the local level of noise perturbation is low. Evaluation of the magnitude and epicentral distance, which are traditionally given by the catalogs, can be difficult, but it is not fully required for κ_r measurement. Indeed, these parameters can be avoided easily by considering a constant f_c equal to that for the earthquake with the lowest magnitude in the catalogs and by neglecting the distance-dependence term for these local events or inferring it through the approximation that R_e is proportional to the travel-time difference $T_S - T_P$ measure for each record.

The κ_{DS} approach has been rarely tested. Previous studies have shown generally higher κ_r and κ_0 with the displacement approach than for the acceleration approach, even though both methods are applied to the same records (Kilb *et al.*, 2012; Ktenidou *et al.*, 2017). Kilb *et al.* (2012) did not observe this tendency for every site, while Ktenidou *et al.* (2017) found a clear and strong discrepancy from very limited bandwidth data recorded in a low-seismicity area. Both studies attributed this to the effects of the smooth transition zone around f_c that is strongly suspected to systematically reduce κ_{r_AS} and increase κ_{r_DS} . Ktenidou *et al.* (2017) showed that measuring κ_{r_DS} below $f_c/2$ (and symmetrically κ_{r_AS} above $2f_c$) greatly reduces this bias. Its influence might be, however, higher for κ_{DS} , because f_c is much more uncertain for low-magnitude events. Here, we found almost the same results for κ_{0_AS} and κ_{0_DS} for the hard-rock sites. In contrast, the results differed greatly for the soil site, although these differences are very likely to be a consequence of site amplification. In the same way, a systematic discrepancy is observed between the m_{κ_DS} and m_{κ_AS} slopes of the distance-dependence linear model, which can be attributed in part to the frequency dependence of the attenuation. However, there is good agreement between m_{κ_DS} and the regional Q values from the literature. The κ_{DS} approach thus appeared to be very well adapted for measurement of κ_0 at rock sites. However, further investigations are required to completely understand what controls the reliability and variability of the κ_{DS} measurement.

Conclusions

The κ parameter is one of the most used and least understood parameters in hazard seismology. This is a clue parameter for host-to-target adjustment, for evaluation of the hazard for hard-rock sites. Site-specific evaluation of κ_0 is essential, although it is generally difficult at the target site in low-to-moderate seismicity areas. This is because the classical approach with acceleration (Anderson and Hough, 1984) requires high-magnitude events to ensure low f_c and good SNR up to high frequencies.

In the present study, the dataset used is based on continuous recordings at two hard-rock sites and one stiff-soil site in Provence, France. These were chosen to carry out site-specific κ determination using the classical Anderson and Hough (1984) approach (κ_{AS}) and the approach proposed by Biasi and Smith (2001; κ_{DS}), which is suitable for low-magnitude events. This evaluation was possible after only a few years of monitoring due to the use of velocimeters, which allowed the recording of much higher numbers of quality events, in comparison with the use of accelerometers. This is particularly true for κ_{DS} , which is measured mainly below 15 Hz, at which accelerometers are less sensitive.

Measuring reliable κ_0 values is not easy, because the physics behind κ is not clear, and the uncertainties associated with this parameter remain high. The choice and the application of the method itself can impact upon the variability of κ . For instance, an important variability is introduced in terms of the operator's subjectivity in the choice of the frequency window used to determine κ_r . To reduce this interoperator variability, a semiautomatic procedure was developed here for the frequency window selection that also has the advantage that it provides the uncertainty associated with each individual κ_r . This uncertainty is shown to be mainly dependent on the width of the frequency window. We observe a systematic shift of every κ_r , due to modifications of the spectrum shape by the site amplification that results in bias for κ_0 , even for rock sites. For some sites, this bias might be strongly frequency dependent and prevent the correct determination of κ_0 . This appears to be the case for the stiff-soil site, where a strong twofold discrepancy is observed between κ_{0_AS} and κ_{0_DS} . Moreover, this frequency-dependent phenomenon increases both the variability of each individual κ_r estimation and the scatter between the κ_r evaluations. The assumption that the attenuation is independent of the frequency made with the definition of κ is questionable. The attenuation is widely accepted to be frequency dependent, at least for its scattering parts. This influence of the scattering on κ cannot be ruled out and might influence both κ_0 and the slope m_κ of the linear dependence on the epicentral distance. However, only an effect on m_κ is observed, through a strong and systematic threefold discrepancy between both of these approaches. The comparison of records from the same cluster of events allows the investigation of the relative effects of the source only. We found that the scatter between the κ_{r_AS} evaluations is clearly and strongly dominated by the source

spectrum variability, whereas the magnitude dependence of κ is suspected but not clearly established.

In the low-to-moderate seismicity context, the κ uncertainty issue is strengthened due to the narrower spectral windows available. Here, there was high impact of the site amplification on κ that led us to discourage its evaluation for soil sites. However, for hard-rock sites that are less affected by site amplification, both the κ_{AS} and κ_{DS} approaches produced consistent results. The site-specific values of κ_0 were around 30 ms (without site amplification correction) for the hard-rock sites in this study area. This value, which is in the upper part of the $\kappa_0 - V_{S30}$ correlation, is consistent with the high attenuation indicated for the Provence region (Mayor *et al.*, 2016) and with the κ_{0_AS} obtained by Douglas *et al.* (2010) for rock sites in the Alps. Moreover, it is in agreement with recent studies that have shown higher κ_0 for hard-rock sites than was initially suggested (Ktenidou *et al.*, 2015; Ktenidou and Abrahamson, 2016; Boore and Campbell, 2017).

The κ_{DS} approach is thus a very promising alternative to the classical approach for sites in a low-to-moderate seismicity context, because this can be carried out using events with smaller magnitudes. This provides a suitable solution for rapid and easy site-specific evaluation of κ_0 , with a potential better accuracy for rock sites than the classical κ_{AS} approach. In the present study, we used a seismicity catalog that might not include the smallest magnitude events. Thus, the κ_{DS} approach can be improved by detection and use of very small and local earthquakes that are not provided by seismic bulletins.

Data and Resources

The seismograms used in this study were collected using a local network that is operated by the French Alternative Energies and Atomic Energy Commission (CEA). Data can be obtained by request to the second author. Earthquake bulletin information was provided mainly by the European-Mediterranean Seismological Centre (<http://www.emsc-csem.org/#2>, last accessed July 2014). If information was missing for an earthquake, information from the Réseau National de Surveillance Sismique (<http://renass.unistra.fr/>, last accessed July 2014), Géoazur (<http://sismoazur.oca.eu/>, last accessed August 2014), or the Italian Seismological Instrumental and Parametric Database (<http://iside.rm.ingv.it/iside/standard/index.jsp>, last accessed August 2014) was used.

Acknowledgments

This study was conducted within the framework of the Cadarache Seismic Hazard Integrated Multidisciplinary Assessment (CASHIMA) Research Program that is funded by the French Alternative Energies and Atomic Energy Commission (CEA), the Laue-Langevin Institute (ILL), and the International Thermonuclear Experimental Reactor (ITER) organization. The authors are thankful to Christopher Berrie and two anonymous reviewers for their careful suggestions and corrections.

References

- Aki, K. (1967). Scaling law of seismic spectrum, *J. Geophys. Res.* **72**, 1217–1231, doi: [10.1029/JZ072i004p01217](https://doi.org/10.1029/JZ072i004p01217).
- Aki, K. (1980). Scattering and attenuation of shear waves in the lithosphere, *J. Geophys. Res.* **85**, 6496–6504, doi: [10.1029/JB085iB11p06496](https://doi.org/10.1029/JB085iB11p06496).
- Aki, K. (1987). Magnitude-frequency relation for small earthquakes: A clue to the origin of f_{\max} of large earthquakes, *J. Geophys. Res.* **92**, 1349–1355.
- Aki, K., and B. Chouet (1975). Origin of coda waves: Source, attenuation, and scattering effects, *J. Geophys. Res.* **80**, 3322–3342.
- Ameri, G., F. Hollender, V. Perron, and C. Martin (2017). Site-specific partially nonergodic PSHA for a hard-rock critical site in southern France: Adjustment of ground motion prediction equations and sensitivity analysis, *Bull. Earthq. Eng.* doi: [10.1007/s10518-017-0118-6](https://doi.org/10.1007/s10518-017-0118-6).
- Anderson, J. G. (1986). Implication of attenuation for studies of the earthquake source, in *Earthquake Source Mechanics*, S. Das, J. Boatwright, and C. H. Scholz (Editors), American Geophysical Union, Washington, D.C., 311–318.
- Anderson, J. G., and S. E. Hough (1984). A model for the shape of the Fourier amplitude spectrum of acceleration at high frequencies, *Bull. Seismol. Soc. Am.* **74**, 1969–1993.
- Anderson, J. G., and J. R. Humphrey (1991). A least squares method for objective determination of earthquake source parameters, *Seismol. Res. Lett.* **62**, 201–209.
- Anderson, J. G., Y. Lee, Y. Zeng, and S. Day (1996). Control of strong motion by the upper 30 meters, *Bull. Seismol. Soc. Am.* **86**, 1749–1759.
- Beresnev, I. A., and G. M. Atkinson (1997). Modeling finite-fault radiation from the omega-n spectrum, *Bull. Seismol. Soc. Am.* **87**, 67–84.
- Biasi, G. P., and K. D. Smith (2001). Site effects for seismic monitoring stations in the vicinity of Yucca Mountain (No. MOL20011204.0045), *A Report Prepared for the U.S. DOE/University and Community College System of Nevada (UCCSN) Cooperative Agreement, Nevada*.
- Boore, D. M. (1986). Short-period *P*- and *S*-wave radiation from large earthquakes: Implications for spectral scaling relations, *Bull. Seismol. Soc. Am.* **76**, 43–64.
- Boore, D. M. (2003). Simulation of ground motion using the stochastic method, *Pure Appl. Geophys.* **160**, 635–676.
- Boore, D. M., and K. W. Campbell (2017). Adjusting central and eastern North America ground-motion intensity measures between sites with different reference-rock site conditions, *Bull. Seismol. Soc. Am.* **107**, 132–148, doi: [10.1785/0120160208](https://doi.org/10.1785/0120160208).
- Borcherdt, R. D. (1970). Effects of local geology on ground motion near San Francisco Bay, *Bull. Seismol. Soc. Am.* **60**, 29–61.
- Brune, J. N. (1970). Tectonic stress and the spectra of seismic shear waves from earthquakes, *J. Geophys. Res.* **75**, 4997–5009.
- Calvet, M., M. Sylvander, L. Margerin, and A. Villaseñor (2013). Spatial variations of seismic attenuation and heterogeneity in the Pyrenees: Coda *Q* and peak delay time analysis, *Tectonophysics* **608**, 428–439, doi: [10.1016/j.tecto.2013.08.045](https://doi.org/10.1016/j.tecto.2013.08.045).
- Campbell, K. W. (2003). Prediction of strong ground motion using the hybrid empirical method and its use in the development of ground-motion (attenuation) relations in eastern North America, *Bull. Seismol. Soc. Am.* **93**, 1012–1033.
- Campbell, K. W. (2004). Erratum to “Prediction of strong ground motion using the hybrid empirical method and its use in the development of ground-motion (attenuation) relations in eastern North America,” *Bull. Seismol. Soc. Am.* **94**, 2418–2418, doi: [10.1785/0120040148](https://doi.org/10.1785/0120040148).
- Campbell, K. W. (2009). Estimates of shear-wave *Q* and θ for unconsolidated and semiconsolidated sediments in eastern North America, *Bull. Seismol. Soc. Am.* **99**, 2365–2392, doi: [10.1785/0120080116](https://doi.org/10.1785/0120080116).
- Cormier, V. F. (1982). The effect of attenuation on seismic body waves, *Bull. Seismol. Soc. Am.* **72**, S169–S200.
- Cotton, F., F. Scherbaum, J. J. Bommer, and H. Bungum (2006). Criteria for selecting and adjusting ground-motion models for specific target regions: Application to central Europe and rock sites, *J. Seismol.* **10**, 137–156, doi: [10.1007/s10950-005-9006-7](https://doi.org/10.1007/s10950-005-9006-7).
- Dainty, A. M. (1981). A scattering model to explain seismic *Q* observations in the lithosphere between 1 and 30 Hz, *Geophys. Res. Lett.* **8**, 1126–1128.
- Delavaud, E., F. Cotton, S. Akkar, F. Scherbaum, L. Danciu, C. Beauval, S. Drouet, J. Douglas, R. Basili, M. A. Sandikkaya, et al. (2012). Toward a ground-motion logic tree for probabilistic seismic hazard assessment in Europe, *J. Seismol.* **16**, 451–473, doi: [10.1007/s10950-012-9281-z](https://doi.org/10.1007/s10950-012-9281-z).
- Douglas, J., P. Gehl, L. F. Bonilla, and C. Gélis (2010). A κ model for mainland France, *Pure Appl. Geophys.* **167**, 1303–1315, doi: [10.1007/s00024-010-0146-5](https://doi.org/10.1007/s00024-010-0146-5).
- Drouet, S., F. Cotton, and P. Guéguen (2010). V_{S30} , κ , regional attenuation and M_w from accelerograms: Application to magnitude 3–5 French earthquakes, *Geophys. J. Int.* **182**, 880–898, doi: [10.1111/j.1365-246X.2010.04626.x](https://doi.org/10.1111/j.1365-246X.2010.04626.x).
- Edwards, B., D. Fäh, and D. Giardini (2011). Attenuation of seismic shear wave energy in Switzerland: Seismic attenuation in Switzerland, *Geophys. J. Int.* **185**, 967–984, doi: [10.1111/j.1365-246X.2011.04987.x](https://doi.org/10.1111/j.1365-246X.2011.04987.x).
- Edwards, B., O.-J. Ktenidou, F. Cotton, N. Abrahamson, C. Van Houtte, and D. Fäh (2015). Epistemic uncertainty and limitations of the κ_0 model for near-surface attenuation at hard rock sites, *Geophys. J. Int.* **202**, 1627–1645, doi: [10.1093/gji/ggv222](https://doi.org/10.1093/gji/ggv222).
- Eva, C., M. Cattaneo, P. Augliera, and M. Pasta (1991). Regional coda *Q* variations in the western Alps (northern Italy), *Phys. Earth Planet. In.* **64**, nos. 1/2, 76–86.
- Futterman, W. I. (1962). Dispersive body waves, *J. Geophys. Res.* **67**, 5279–5291, doi: [10.1029/JZ067i013p05279](https://doi.org/10.1029/JZ067i013p05279).
- Gariel, J.-C., and M. Campillo (1989). The influence of the source on the high-frequency behavior of the near-field acceleration spectrum: A numerical study, *Geophys. Res. Lett.* **16**, 279–282.
- Garofalo, F., S. Foti, F. Hollender, P. Y. Bard, C. Cornou, B. R. Cox, A. Dechamp, M. Ohrmberger, V. Perron, D. Sicilia, et al. (2016). InterPA-CIFIC project: Comparison of invasive and non-invasive methods for seismic site characterization. Part II: Inter-comparison between surface-wave and borehole methods, *Soil Dynam. Earthq. Eng.* **82**, 241–254, doi: [10.1016/j.soildyn.2015.12.009](https://doi.org/10.1016/j.soildyn.2015.12.009).
- Graves, R. W., and A. Pitarka (2010). Broadband ground-motion simulation using a hybrid approach, *Bull. Seismol. Soc. Am.* **100**, 2095–2123, doi: [10.1785/0120100057](https://doi.org/10.1785/0120100057).
- Guéguen, P., C. Cornou, S. Garambois, and J. Banton (2007). On the limitation of the H/V spectral ratio using seismic noise as an exploration tool: Application to the Grenoble Valley (France), a small apex ratio basin, *Pure Appl. Geophys.* **164**, 115–134, doi: [10.1007/s00024-006-0151-x](https://doi.org/10.1007/s00024-006-0151-x).
- Hanks, T. C. (1982). f_{\max} , *Bull. Seismol. Soc. Am.* **72**, 1867–1879.
- Hough, S. E., and J. G. Anderson (1988). High-frequency spectra observed at Anza, California: Implications for *Q* structure, *Bull. Seismol. Soc. Am.* **78**, 692–707.
- Hough, S. E., J. G. Anderson, J. Brune, E. Vernon, J. Berger, J. Fletcher, L. Haar, L. Hanks, and L. Baker (1988). Attenuation near Anza, California, *Bull. Seismol. Soc. Am.* **78**, 672–691.
- Hough, S. E., J. M. Lees, and E. Monastero (1999). Attenuation and source properties at the Coso Geothermal Area, California, *Bull. Seismol. Soc. Am.* **89**, 1606–1619.
- Kennett, B. L. N. (1974). Reflections, rays, and reverberations, *Bull. Seismol. Soc. Am.* **64**, 1685–1696.
- Kilb, D., G. Biasi, J. Anderson, J. Brune, Z. Peng, and F. L. Vernon (2012). A comparison of spectral parameter kappa from small and moderate earthquakes using southern California ANZA seismic network data, *Bull. Seismol. Soc. Am.* **102**, 284–300, doi: [10.1785/0120100309](https://doi.org/10.1785/0120100309).
- Knopoff, L. (1964). *Q*, *Rev. Geophys. Space Phys.* **2**, 625–660.
- Konno, K., and T. Ohmachi (1998). Ground-motion characteristics estimated from spectral ratio between horizontal and vertical components of microtremor, *Bull. Seismol. Soc. Am.* **88**, 228–241.
- Kottke, A. R. (2017). V_{S30} - κ_0 relationship implied by ground motion models? *16th World Conference on Earthquake Engineering (16WCEE)*, Santiago Chile, 9–13 January, Paper Number 3089.

- Ktenidou, O.-J., and N. A. Abrahamson (2016). Empirical estimation of high-frequency ground motion on hard rock, *Seismol. Res. Lett.* doi: [10.1785/0220160075](https://doi.org/10.1785/0220160075).
- Ktenidou, O.-J., N. A. Abrahamson, S. Drouet, and F. Cotton (2015). Understanding the physics of kappa (κ): Insights from a downhole array, *Geophys. J. Int.* **203**, 678–691, doi: [10.1093/gji/ggv315](https://doi.org/10.1093/gji/ggv315).
- Ktenidou, O.-J., F. Cotton, N. A. Abrahamson, and J. G. Anderson (2014). Taxonomy of kappa: A review of definitions and estimation approaches targeted to applications, *Seismol. Res. Lett.* **85**, 135–146, doi: [10.1785/0220130027](https://doi.org/10.1785/0220130027).
- Ktenidou, O.-J., C. Gélis, and L.-F. Bonilla (2013). A study on the variability of kappa in a borehole: Implications of the computation process, *Bull. Seismol. Soc. Am.* **103**, 1048–1068, doi: [10.1785/0120120093](https://doi.org/10.1785/0120120093).
- Ktenidou, O.-J., W. J. Silva, R. B. Darragh, N. A. Abrahamson, and T. Kishida (2017). Squeezing kappa (κ) out of the transportable array: A strategy for using bandlimited data in regions of sparse seismicity, *Bull. Seismol. Soc. Am.* **107**, 256–275, doi: [10.1785/0120150301](https://doi.org/10.1785/0120150301).
- Kudo, K. (1995). Practical estimates of site response. State-of-the-art report, *Proc. of the Fifth International Conference on Seismic Zonation*, Nice, France, 17–19 October.
- Laurendeau, A., P.-Y. Bard, F. Hollender, V. Perron, L. Foundotos, O.-J. Ktenidou, and B. Hernandez (2017). Derivation of consistent hard rock ($1000 < V_S < 3000$ m/s) GMPEs from surface and down-hole recordings: Analysis of KiK-net data, *Bull. Earthq. Eng.* 1–32, doi: [10.1007/s10518-017-0142-6](https://doi.org/10.1007/s10518-017-0142-6).
- Laurendeau, A., F. Cotton, O.-J. Ktenidou, L.-F. Bonilla, and F. Hollender (2013). Rock and stiff-soil site amplification: Dependency on V_{S30} and kappa (κ_0), *Bull. Seismol. Soc. Am.* **103**, 3131–3148, doi: [10.1785/0120130020](https://doi.org/10.1785/0120130020).
- Lermo, J., and F. J. Chávez-García (1993). Site effect evaluation using spectral ratios with only one station, *Bull. Seismol. Soc. Am.* **83**, 1574–1594.
- Maufroy, E., V. M. Cruz-Atienza, F. Cotton, and S. Gaffet (2015). Frequency-scaled curvature as a proxy for topographic site-effect amplification and ground-motion variability, *Bull. Seismol. Soc. Am.* **105**, 354–367, doi: [10.1785/0120140089](https://doi.org/10.1785/0120140089).
- Mayor, J., M. Calvet, L. Margerin, O. Vanderhaeghe, and P. Traversa (2016). Crustal structure of the Alps as seen by attenuation tomography, *Earth Planet. Sci. Lett.* **439**, 71–80, doi: [10.1016/j.epsl.2016.01.025](https://doi.org/10.1016/j.epsl.2016.01.025).
- Nakamura, Y. (1989). A method for dynamic characteristics estimation of subsurface using microtremor on the ground surface, *Q. Rep. Railway Tech. Res. Inst.* **30**, 25–33.
- Papageorgiou, A. S. (1988). On two characteristic frequencies of acceleration spectra: Patch corner frequency and f_{\max} , *Bull. Seismol. Soc. Am.* **78**, 509–529.
- Papageorgiou, A. S. (2003). The barrier model and strong ground motion, *Pure Appl. Geophys.* **160**, 603–634.
- Papageorgiou, A. S., and K. Aki (1983). A specific barrier model for the quantitative description of inhomogeneous faulting and the prediction of strong ground motion: Part II. Applications of the model, *Bull. Seismol. Soc. Am.* **73**, 953–978.
- Parolai, S., and D. Bindi (2004). Influence of soil-layer properties on κ evaluation, *Bull. Seismol. Soc. Am.* **94**, 349–356.
- Parolai, S., D. Bindi, and M. Pilz (2015). κ_0 : The role of intrinsic and scattering attenuation, *Bull. Seismol. Soc. Am.* **105**, 1049–1052, doi: [10.1785/0120140305](https://doi.org/10.1785/0120140305).
- Perron, V., A. Laurendeau, F. Hollender, P.-Y. Bard, C. Gélis, P. Traversa, and S. Drouet (2017). Selecting time windows of seismic phases and noise for engineering seismology applications: A versatile methodology and algorithm, *Bull. Earthq. Eng.* doi: [10.1007/s10518-017-0131-9](https://doi.org/10.1007/s10518-017-0131-9).
- Pilz, M., and D. Fäh (2017). The contribution of scattering to near-surface attenuation, *J. Seismol.* **21**, 837–855, doi: [10.1007/s10950-017-9638-4](https://doi.org/10.1007/s10950-017-9638-4).
- Purvanche, M. D., and J. G. Anderson (2003). A comprehensive study of the observed spectral decay in strong-motion accelerations recorded in Guerrero, Mexico, *Bull. Seismol. Soc. Am.* **93**, 600–611.
- Rovelli, A. (1982). On the frequency dependence of Q in Friuli from short period digital records, *Bull. Seismol. Soc. Am.* **72**, 2369–2372.
- Sanchez, G., Y. Rolland, D. Schreiber, G. Giannerini, M. Corsini, and J.-M. Lardeaux (2010). The active fault system of SW Alps, *J. Geodyn.* **49**, 296–302.
- Steidl, J. H., A. G. Tumarkin, and R. J. Archuleta (1996). What is a reference site? *Bull. Seismol. Soc. Am.* **86**, 1733–1748.
- Thouvenot, F. (1983). Frequency dependence of the quality factor in the upper crust: A deep seismic sounding approach, *Geophys. J. Int.* **73**, 427–447.
- Tsai, C.-C. P., and K.-C. Chen (2000). A model for the high-cut process of strong-motion accelerations in terms of distance, magnitude, and site condition: An example from the SMART 1 array, Lotung, Taiwan, *Bull. Seismol. Soc. Am.* **90**, 1535–1542.
- Van Houtte, C., S. Drouet, and E. Cotton (2011). Analysis of the origins of κ (kappa) to compute hard rock to rock adjustment factors for GMPEs, *Bull. Seismol. Soc. Am.* **101**, 2926–2941, doi: [10.1785/0120100345](https://doi.org/10.1785/0120100345).
- Van Houtte, C., O.-J. Ktenidou, T. Larkin, and C. Holden (2014). Hard-site κ_0 (kappa) calculations for Christchurch, New Zealand, and comparison with local ground-motion prediction models, *Bull. Seismol. Soc. Am.* **104**, 1899–1913, doi: [10.1785/0120130271](https://doi.org/10.1785/0120130271).
- Warren, N. (1972). Q and structure, *The Moon* **4**, 430–441, doi: [10.1007/BF00562009](https://doi.org/10.1007/BF00562009).
- Wen, J., and X. Chen (2012). Variations in f_{\max} along the ruptured fault during the M_w 7.9 Wenchuan earthquake of 12 May 2008, *Bull. Seismol. Soc. Am.* **102**, 991–998, doi: [10.1785/0120110105](https://doi.org/10.1785/0120110105).
- French Alternative Energies and Atomic Energy Commission (CEA),
Cadarache, DPIE/SA2S, DEN
Bât. 352
F-13108 Saint-Paul-lez-Durance
France
vincent.perron.mail@gmail.com
(V.P., F.H., C.G.-B.)
- University of Grenoble Alpes
ISTerre, CNRS, IRD, IFSTTAR
F-38000 Grenoble
France
(P.-Y.B.)
- IRSN, PRP-DGE/SCAN/BERSSIN
BP 17
F-92262 Fontenay-aux-Roses
France
(C.G.)
- CEA, DIF
F-91297 Arpajon
France
(B.H.)
- Department of Engineering Science
University of Greenwich
Central Avenue, Chatham Maritime
Kent ME4 4TB, United Kingdom
(O.-J.K.)